RING RESONATOR METHOD FOR

DIELECTRIC PERMITTIVITY MEASUREMENT OF FOAMS

by

Isaac Waldron

A Thesis

Submitted to the Faculty

of the

WORCESTER POLYTECHNIC INSTITUTE

in partial fulfillment of the requirements for the

Degree of Master of Science

in

Electrical and Computer Engineering

May 3rd, 2006

Approved by:

_____   _____

Sergey Makarov   Reinhold Ludwig
Thesis Advisor   Thesis Committee
ECE Department   ECE Department

_____

Scott Biederman
Thesis Committee
General Motors

Abstract

Dielectric permittivity measurements provide important input to engineering and scientific disciplines due to the effects of permittivity on the interactions between electromagnetic energy and materials. A novel ring resonator design is presented for the measurement of permittivity of low dielectric constant foams. A review of dielectric material properties and currently available measurement methods is included. Measurements of expanded polystyrene are reported and compared with results from the literature; good agreement between measurements and published results is shown.

Acknowledgements

Table of Contents

List of Tables

List of Figures

1. Introduction

Due to their influence on the interaction of electromagnetic energy with materials, dielectric properties of materials are useful data for imaging and radar experimentation. In particular, the dielectric properties of expanded polystyrene (EPS) foams are interesting as they drive the use of EPS foams as physical supports for radar cross-section measurements and other applications. These foams are also utilized in modern antenna research as supporting materials for antenna construction and for radomes. Electromagnetic imaging applications require the dielectric properties of materials to predict the interaction between fields used for imaging and the materials. Few examples are available of research directed at the measurement of foam permittivity, or dielectric constant and loss tangent.

In this thesis, I describe a new microstrip-based resonant device that is specifically intended for permittivity measurements of low dielectric constant materials at frequencies 1 to 10 GHz. The device is based on a microstrip ring resonator with the ring and the ground plane/feed network physically located in *separate* planes. This enables the placement of an arbitrary sample of material to be measured between the ring resonator and ground plane. A transmission line method (TLM) is used to predict the frequency response including feed and radiation effects. Experimental data in L- and S-bands are presented and compared with theory estimates for the foams.

2. Background

The dielectric properties of materials are important inputs to a great deal of engineering and scientific work in electrical engineering. They define the interaction between static or dynamic electric and magnetic fields and the materials that make up the world around us. As a result, there are many sources of information regarding the definition and measurement of dielectric properties in the engineering literature. In this section, I give an overview of dielectric material properties and summarize both U.S. patents and selected items from the literature as they relate to dielectric measurement.

2.1. Dielectric Properties of Materials

In most dielectric materials, the electric field and electric flux density are related by a simple relationship:

$$\mathbf{D} = \varepsilon\mathbf{E} \tag{1}$$

where ε, the permittivity of the dielectric material, is a constant with the units of F/m. Materials for which (1) applies are linear and isotropic. In general, for such materials ε can be temperature and frequency dependent. As a first-order approximation for applications without wide temperature or frequency limits, ε is a constant complex quantity that can be broken into two components ε_r and $\tan\delta$:

$$\varepsilon = \varepsilon_0\varepsilon_r\left(1 - j\tan\delta\right) \tag{2}$$

where $\varepsilon_0 = 8.854 \times 10^{-12}$ is the permittivity of free space. When expressed in this form, ε_r and $\tan\delta$ are called the dielectric constant loss tangent of the material. In the case where $\tan\delta$ is small, on the order of 10^{-2} or less, the speed at which electromagnetic energy propagates through a medium, v_p, is given by

$$v_p = \frac{c}{\sqrt{\varepsilon_r}} \qquad (3)$$

where $c = 2.988 \times 10^8$ m/s is the speed of light in a vacuum. The loss tangent $\tan\delta$ exhibits how strongly energy is absorbed by a medium. In a homogenous medium, a plane wave traveling along the z-axis and with the electric field oriented in the xz-plane is described by

$$E_x(z) = E^+ e^{-\gamma z} + E^- e^{+\gamma z} \qquad (4)$$

where E^+ and E^- are arbitrary amplitude constants and γ is the propagation constant for the medium defined by

$$\gamma = \alpha + j\beta = j\omega\sqrt{\mu_0 \varepsilon_0 \varepsilon_r (1 - j\tan\delta)} \qquad (5)$$

where $\mu_0 = 4\pi \times 10^{-7}$ is the permeability of free space.

The propagation constant γ has another effect on wave propagation that is important for imaging considerations. The propagation constant affects the intrinsic impedance, η, of the material:

$$\eta = \frac{j\omega\mu}{\gamma} = \sqrt{\frac{\mu}{\varepsilon}} \qquad (6)$$

When a traveling wave encounters an interface between materials with differing intrinsic impedances, some of the energy is reflected at the interface and the remainder crosses the interface into the new material. The reflection and transmission coefficients, denoted Γ and T, for normal incidence of a plane wave are

$$\Gamma = \frac{\eta_2 - \eta_1}{\eta_2 + \eta_1} \qquad (7)$$

$$T = \frac{2\eta_2}{\eta_2 + \eta_1} \qquad (8)$$

where η_1 is the intrinsic impedance of the medium in which the incident wave starts and η_2 is the intrinsic impedance of the medium in which the wave is transmitted.

The material properties dielectric constant and loss tangent play important roles in the propagation of electromagnetic energy in dielectric media. In a low-loss case, the dielectric constant ε_r slows the propagation of energy through a media by altering the phase velocity. The loss tangent $\tan\delta$ specifies how much energy is absorbed as a wave travels through a medium. The propagation constant, which takes ε_r and $\tan\delta$ as parameters, defines the intrinsic impedance of the medium and the behavior of waves at the interfaces between different media.

2.2. Dielectric Properties of EPS Foams

There is a dearth of directly measured data of dielectric permittivities of expanded polystyrene (EPS) foams. Treatment in the literature is generally confined to theoretical predictions and indirect results from radar cross-section (RCS) studies. Reported measurements vary over a small range for both bulk and expanded polystyrene.

In a seminal paper published in January 1965, M. Plonus established a theory for predicting the RCS of EPS foam supports used for radar measurements [1]. In this paper, Plonus models EPS foam as a collection of "randomly arranged, closely packed spherical shells." He finds the volume ratio of air to polystyrene in the foam as a function of foam density and uses this to determine the dielectric constant of the foam. For an air-blown EPS foam of density 26 kg/m^3 Plonus concludes a dielectric constant of 1.04 [1].

E. F. Knott in August 1993 published his model of plastic foams as a regular cubic lattice [2]. Knott derives the dielectric constant of a foam from the capacitance of a unit cell of the cubic lattice model. Ultimately, he provides a formula based on the dielectric constants of the base polymer and inclusion gas and the volumetric fraction of polymer in the foam. For an air-blown

foam of density 26 kg/m^3 Knott's formula predicts a dielectric constant of 1.03. He compares his result to a logarithmic prediction of dielectric constant by Cuming as well as dielectric constants derived from backscatter measurements of extruded polystyrene forms.

2.3. Measurement Methods for the Dielectric Constant

Knowledge of the dielectric constant, ε_r, and loss tangent, tan δ, of a dielectric material is required to understand how that material will react to electromagnetic fields and behave in RF circuits. A variety of techniques are available to measure these properties, including methods based on free-space, waveguide, and resonator measurements. These techniques have been described in both the scientific literature and in United States utility patents. This section is a review of the available literature.

U.S. Patent 3,965,416, issued June 22, 1976, describes a method of dielectric constant measurement using a pulse delay oscillator [7]. The material under test is used to alter the phase velocity of signals traveling along a shorted transmission line. This transmission line is the frequency determining component of the pulse delay oscillator, and so the frequency of oscillation is used to calculate the phase velocity.

U.S. Patent 5,132,623, issued July 21, 1992, describes a broadband dielectric property measurement technique specifically applied to the problem of oil-bearing strata determination [8]. The apparatus described consists of broadband transmitting and receiving antennas which are used to measure dielectric constant from frequency- or time-domain methods. The inventors claim a measurement frequency range of 2 kHz-1 GHz.

U.S. Patent 5,157,337, issued October 20, 1992, describes a probe for dielectric constant measurements of thin materials [9]. The device is essentially a resonator constructed from an open coaxial transmission line. Fringing fields from the open end of the resonator penetrate into

the material under test, and the resonant frequency is affected by the dielectric constant of that material. The inventors claim accuracy of better than one percent.

U.S. Patent 6,496,018, issued December 17, 2002, describes a method for determining a calibration curve for an open, or radiating, resonator that relates the resonant frequency to the dielectric constant and thickness of a sheet of sample material of known dielectric constant [10]. This calibration curve is then applied to find the dielectric constant of a material with unknown properties.

Free-space methods for measuring dielectric constant rely primarily on reflection and transmission of electromagnetic waves through a sample of the material under test. Reference [11] describes a method using dielectric lenses to focus a signal on a small piece of material under test. The dielectric constant and loss tangent are then found from the scattering parameters of the complete system. The authors of [12] use a similar experimental setup to that of [11], but establish a relation between the reflection coefficient and the complex permittivity of the material under test to determine dielectric constant and loss tangent. Reference [13] describes a method to measure the properties of large slabs of material using two standard horn antennas. The authors also use some algebraic manipulation to reduce the problem from a 2-D search of a complex space to a search on a real-valued function.

Waveguide methods for dielectric property measurement involve the comparison of empty waveguide with a waveguide including the sample material or the comparison of measured scattering parameters and numerical electromagnetic solutions. The waveguide may be either fully or partially filled with the material under test. In [14], the material under test partially fills a shorted waveguide and the measured reflection coefficient is compared to a FEM solution of the system. The authors of [15] fit an expression for the effective complex dielectric constant to

measurements of a system composed of two rectangular waveguides separated by a relatively thin piece of sample material. In [16] the complex permittivity of a cylindrical rod is calculated from the resonant frequency and bandwidth of the transmission spectrum. The authors of [17] measure the reflection coefficient of a thin sample in a matched waveguide and compare to a model of the system using an infinitesimally thin resistive sheet as the sample.

The literature contains many papers dedicated to resonator structures. Methods for measuring dielectric properties using waveguide cavities [18]-[20], ring resonators [21]-[23], microstrip resonators [24]-[25], and dielectric resonators [26]-[27] have been reported. Other papers have focused on the modeling of ring resonators [28]-[29] or on modified resonator structures [30]. A special class of resonator-based methods contains those based on the use of antennas [31]-[35]. The methods for measuring dielectric properties using resonators are well developed and most use the scattering parameters of a one- or two-port resonator system as a basic measurement. These measurements are then compared with numerical or analytical solutions of the system to find the dielectric constant and loss tangent values. Of interest is a paper that uses a large open resonator with a multilayered dielectric load to determine the properties of an unknown layer in the load [34]. The authors develop an analytical formula for the loss tangent of an unknown sample material. The technique is aimed at the measurement of high-permittivity layers in multilayer systems.

The techniques presented in this section have varying applicability to the determination of EPS foam permittivity. In general, the full-wave methods will be very computationally intensive, while the methods based on perturbation of a resonant cavity will require standards of known dielectric constant and loss tangent to calibrate against. Therefore, there exists a need for

a reasonably accurate method that neither is computationally intensive nor requires samples of known permittivity for calibration.

3. Theoretical Basis

In this section I present a theoretical analysis for a ring resonator-based method for the measurement of complex dielectric permittivity of materials. First I present the theory for a planar ring and feed structure, and then I extend the theory to a case with the ring in a parallel plane above the feeding plane. Finally, I explain how raw measurements of the ring and feed structure can be processed to determine the complex permittivity of a material.

3.1. Ring Resonator Method

A ring resonator structure on a printed circuit board (PCB) can be used to determine the complex permittivity of the substrate material. Similar to the methods presented in [21]-[23], I use a measurement of the S_{21} parameter of a two-port ring resonator to determine the permittivity of the board substrate.

3.1.1. Structure

The ring resonator device consists entirely of printed microstrips on a rigid substrate. A two-layer board with one dielectric material is used, as shown in Fig. 1. Fig. 1a shows the relative positions of the ring and feed lines on the upper surface of the board, and Fig. 1b shows a side view of the board in which the ground plane is visible. The ground plane occupies the entire lower surface of the board. The feed lines and ring resonator are printed transmission lines with width chosen for 50 Ω characteristic impedance. A small gap Δ is included between the ring and each feed line; this gap is included to separate the resonant behavior of the ring from the feed network and ranges from 0.1 to 1.0 times the width of the feed microstrip. SMA connectors, shown on the left and right sides of Fig. 1a, are used to connect the device to a network analyzer for measurement.
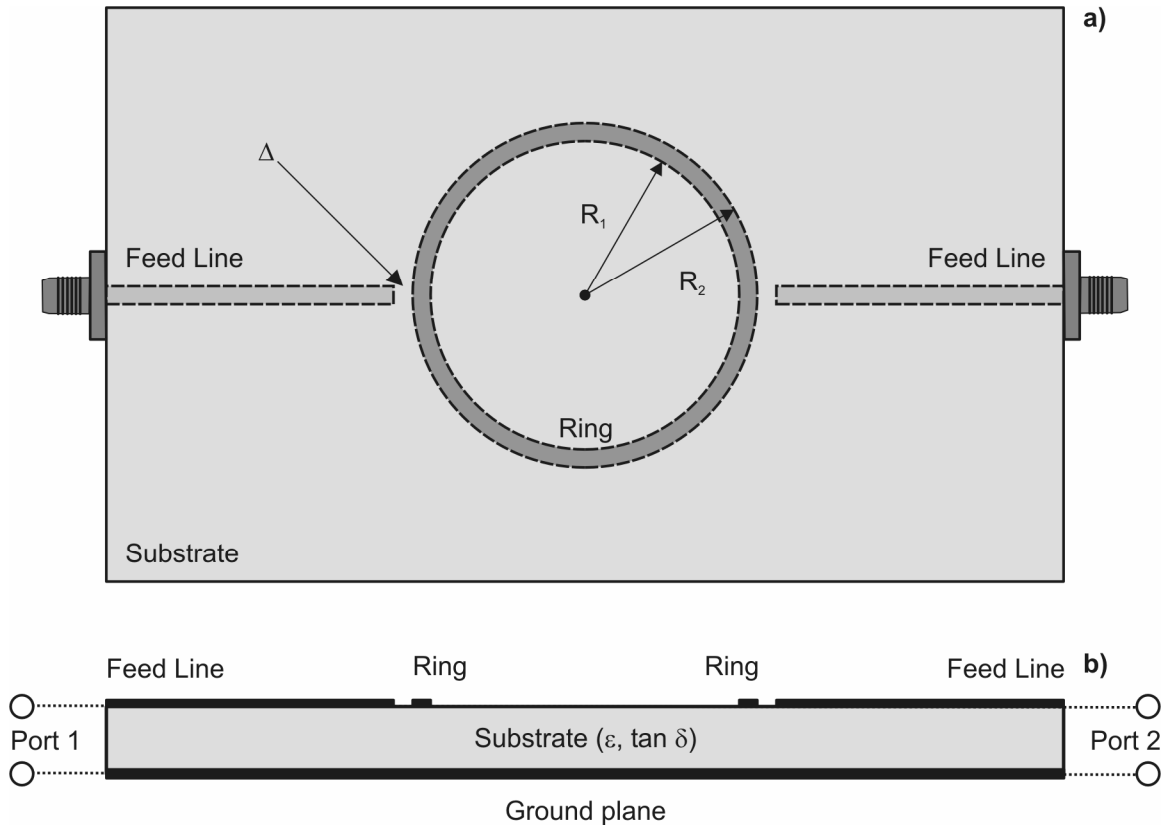
Fig. 1 Planar ring resonator for measurement of RF substrate shown from a) top and b) side views.

3.1.2. Network Parameter Formulation

The device shown in Fig. 1 is represented as a network circuit as shown in Fig. 2. Each shaded box in Fig. 2 is a separately modeled circuit element, and the overall network parameters of the device are found from the combination of these elements in cascade. The feed lines, which are approximately lossless and matched to 50 Ω, are not considered in this model because it is possible to determine the permittivity of the substrate using only the magnitude of the S_{21} parameter.

Fig. 2 Network circuit of planar ring resonator.

Each of the circuit elements in Fig. 2 is represented by its network parameters in any one of several formulations [36],[37]. A representation of a circuit element in one formulation can be converted into a representation of that element in any other formulation using a straightforward set of algebraic rules, such as those in Table 4-2 of [36] and Table 4.2 of [37]. This speeds the analysis of network circuits as some formulations are particularly suited for particular combinations of elements. For example, admittance parameters, also called Y-parameters, are useful because parallel combinations of elements are accomplished by simply adding the Y-parameter matrices for the elements.

Ultimately, each element of Fig. 2 is represented in the ABCD parameter formulation of the network parameters. In this formulation, the response of a system can be simply calculated as the product of the ABCD parameter matrices of cascaded elements. The development of the ABCD matrices for particular elements is described in the below sections.

3.1.3. Gap Model

As shown in Fig. 1, there is a small gap of width Δ between each feed line and the ring resonator. This gap slightly affects the resonant frequencies of the ring resonator but greatly affects the peak amplitudes of the S_{21} parameter of the device. In order to take these effects into account, an equivalent circuit for the gap must be included in the description of the device. In Fig. 2, the boxes labeled "Left Gap" and "Right Gap" are modeled as a pair of capacitors as shown in Fig. 3. Each gap is modeled by a parasitic capacitor C_p and a gap capacitance C_g, following the work of Yu and Chang in [28].
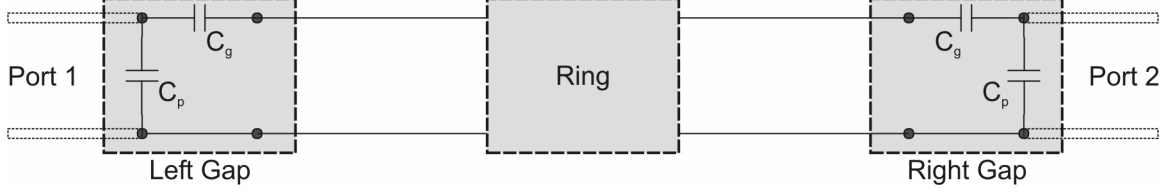
Fig. 3 Network circuit of planar ring resonator with gap model detail.

The capacitor values are found by closed-form expressions of Garg and Bahl [38] as modified by Yu and Chang [28]:

$$\frac{C_{\text{even}}(\varepsilon_r = 9.6)}{W} = 12\left(\frac{\Delta}{W}\right)^{m_e} e^{k_e} \text{ (pF/m)} \tag{9}$$

$$\frac{C_{\text{odd}}(\varepsilon_r = 9.6)}{W} = \left(\frac{\Delta}{W}\right)^{m_0} e^{k_0} \text{ (pF/m)} \tag{10}$$

$$m_e = 0.8675, k_e = 2.043\left(\frac{W}{h}\right)^{0.12}, 0.1 \le \frac{\Delta}{W} \le 0.5 \tag{11}$$

$$m_e = \frac{1.565}{\left(\frac{W}{h}\right)^{0.16}} - 1, k_e = 1.97 - \frac{0.03}{\left(\frac{W}{h}\right)}, 0.5 \le \frac{\Delta}{W} \le 1.0 \tag{12}$$

$$m_0 = \frac{W}{h}\left(0.619\log_{10}\frac{W}{h} - 0.3853\right), k_0 = 4.26 - 1.453\log_{10}\frac{W}{h}, 0.1 \le \frac{\Delta}{W} \le 1.0 \tag{13}$$

$$C_{\text{even}}(\varepsilon_r) = 1.167 C_{\text{even}}(\varepsilon_r = 9.6)\left(\frac{\varepsilon_r}{9.6}\right)^{0.9} \tag{14}$$

$$C_{\text{odd}}(\varepsilon_r) = 1.1 C_{\text{odd}}(\varepsilon_r = 9.6)\left(\frac{\varepsilon_r}{9.6}\right)^{0.8} \tag{15}$$

$$C_p = \frac{C_{\text{even}}(\varepsilon_r)}{2} \tag{16}$$

$$C_g = \frac{2C_{\text{odd}}(\varepsilon_r) - C_{\text{even}}(\varepsilon_r)}{4} \tag{17}$$

where W is the width of the feed line, Δ is the width of the gap, and h is the thickness of the feed line substrate. The two capacitors are then combined into ABCD parameter formulations for the left and right gaps using Table 4-1 of [36] and matrix arithmetic:

$$[ABCD]_{C_p} = \begin{bmatrix} 1 & 0 \\ j\omega C_p & 1 \end{bmatrix} \tag{18}$$

$$[ABCD]_{C_g} = \begin{bmatrix} 1 & \dfrac{1}{j\omega C_g} \\ 0 & 1 \end{bmatrix} \tag{19}$$

$$[ABCD]_{\text{left}} = [ABCD]_{C_p}[ABCD]_{C_g} = \begin{bmatrix} 1 & \dfrac{1}{j\omega C_g} \\ j\omega C_p & 1 \end{bmatrix} \tag{20}$$

$$[ABCD]_{\text{right}} = [ABCD]_{C_g}[ABCD]_{C_p} = \begin{bmatrix} 1 + \dfrac{C_p}{C_g} & \dfrac{1}{j\omega C_g} \\ j\omega C_p & 1 \end{bmatrix} \tag{21}$$

3.1.4. Ring Resonator Model

My analysis of the ring resonator, the box labeled "Ring" in Fig. 2 and Fig. 3, also follows the work of Yu and Chang. In [28], they cite a previous work by Owens that concludes that curvature effects can be ignored for microstrip ring resonators of sufficiently large diameter as compared to their width [39]. In this case, Yu and Chang point out that a microstrip ring resonator of large diameter can be modeled as two straight sections of microstrip that are connected in parallel. The parallel configuration of microstrips is shown in schematic form in Fig. 4.
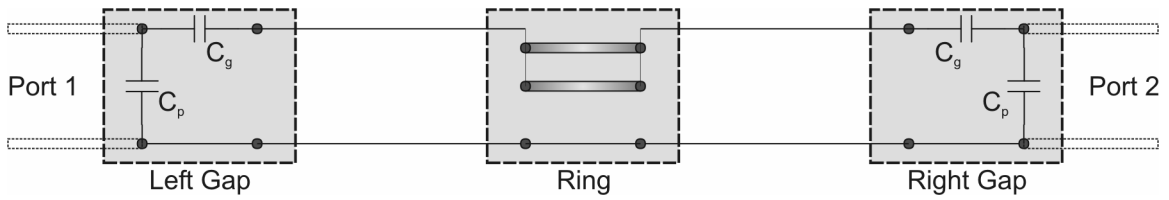
Fig. 4 Network circuit of planar ring resonator with gap and ring model detail.

Analysis of the ring structure begins with the representation of each half-ring microstrip section in the S parameter formulation:

$$[S]_{\text{half-ring}} = \begin{bmatrix} 0 & e^{-\pi\gamma R_m} \\ e^{-\pi\gamma R_m} & 0 \end{bmatrix} \tag{22}$$

18

where γ is the complex propagation constant along the ring microstrip and R_m is the mean radius of the ring. The propagation constant γ is given by

$$\gamma = j\omega\sqrt{\mu_0\varepsilon_0\varepsilon_e(1-j\tan\delta)} \tag{23}$$

where ε_e is the effective dielectric constant of the microstrip ring dependent on the ring width W, substrate thickness h, and substrate dielectric constant ε_r. ε_e is found by applying a formula found in both [40] and [41] for the appropriate value of the ratio of W to h:

$$\varepsilon_e = \frac{\varepsilon_r+1}{2} + \frac{\varepsilon_r-1}{2}\left[\left(1+12\frac{h}{W}\right)^{-\frac{1}{2}} + 0.04\left(1-\frac{W}{h}\right)^2\right], \frac{W}{h} < 1 \tag{24}$$

$$\varepsilon_e = \frac{\varepsilon_r+1}{2} + \frac{\varepsilon_r-1}{2}\left(1+12\frac{h}{W}\right)^{-\frac{1}{2}}, \frac{W}{h} \geq 1 \tag{25}$$

Since the feed points lie on a diameter of the ring as shown in Fig. 1, the S parameters for each half-ring are identical. The S parameters for the half-ring sections are converted to the Y parameter formulation, in which the parallel combination of elements is represented by addition:

$$[Y]_{\text{half-ring}} = \frac{1}{Z_0\left(e^{-2\pi\gamma R_m}-1\right)}\begin{bmatrix} -1-e^{-2\pi\gamma R_m} & 2e^{-\pi\gamma R_m} \\ 2e^{-\pi\gamma R_m} & -1-e^{-2\pi\gamma R_m} \end{bmatrix} \tag{26}$$

$$[Y]_{\text{ring}} = \frac{2}{Z_0\left(e^{-2\pi\gamma R_m}-1\right)}\begin{bmatrix} -1-e^{-2\pi\gamma R_m} & 2e^{-\pi\gamma R_m} \\ 2e^{-\pi\gamma R_m} & -1-e^{-2\pi\gamma R_m} \end{bmatrix} \tag{27}$$

where Z_0 is the characteristic impedance of the microstrip transmission line that forms the ring. The Y parameter formulation is then converted to the ABCD parameter formulation:

$$[ABCD]_{\text{ring}} = \begin{bmatrix} \dfrac{e^{\pi\gamma R_m}+e^{-\pi\gamma R_m}}{2} & \dfrac{Z_0\left(e^{\pi\gamma R_m}-e^{-\pi\gamma R_m}\right)}{4} \\ \dfrac{e^{\pi\gamma R_m}-e^{-\pi\gamma R_m}}{Z_0} & \dfrac{e^{\pi\gamma R_m}+e^{-\pi\gamma R_m}}{2} \end{bmatrix} \tag{28}$$

3.1.5. Complete Device Model

As mentioned above, the overall response of the device is calculated by the products of the ABCD parameter matrices of the individual elements. The ABCD matrix of the system in Fig. 2 is then

$$[ABCD]_{\text{device}} = [ABCD]_{\text{left}}[ABCD]_{\text{ring}}[ABCD]_{\text{right}} \qquad (29)$$

This ABCD matrix can be converted to the S parameter formulation to completely describe the operation of the device in a form that will match that measured by a vector network analyzer.

$$S_{21} = \frac{2}{A + \dfrac{B}{Z_0} + Z_0 C + D}$$

$$= \frac{8Z_0^2 C_g^2 e^{-\gamma L} \omega^2}{\begin{aligned} &4\left(e^{-2\gamma L} - 1\right) + j4Z_0\omega\left[-3C_g - 2C_p + \left(C_g + 2C_p\right)e^{-2\gamma L}\right] + \\ &Z_0^2\omega^2\left[9C_g^2 + 4C_p^2 + 16C_g C_p - \left(C_g^2 + 4C_p^2\right) - 3C_g - 2C_p + \left(C_g^2 + 4C_p^2\right)e^{-2\gamma L}\right] + \\ &j2Z_0^3 C_g C_p\omega^3\left[3C_g + 2C_p + \left(C_g + 2C_p\right)e^{-2\gamma L}\right] + Z_0^4 C_g^2 C_p^2\omega^4\left(e^{-2\gamma L} - 1\right) \end{aligned}} \qquad (30)$$

where Z_0 is the characteristic impedance of the microstrip ring calculated from formulas in [40] and [41]:

$$Z_0 = \frac{Z_f}{2\pi\sqrt{\varepsilon_e}}\ln\left(\frac{8h}{W} + \frac{W}{4h}\right), \frac{W}{h} < 1 \qquad (31)$$

$$Z_0 = \frac{Z_f}{\sqrt{\varepsilon_e}\left(1.393 + \dfrac{W}{h} + \dfrac{2}{3}\ln\left(\dfrac{W}{h} + 1.444\right)\right)}, \frac{W}{h} \geq 1 \qquad (32)$$

where Z_f is 376.8 Ω, the characteristic impedance of free space.

3.2. Suspended Ring Resonator Method

Unfortunately, the device shown in Fig. 1 cannot be used to measure the dielectric permittivities of polymer foams due to the difficulty of printing circuits on foams. The field of the microstrip ring is concentrated in the dielectric substrate below and around the ring. In order

to exploit this concentration of field, I propose a suspended ring resonator structure that places material to be measured between the microstrip ring and the ground plane. This ensures that the resonator is strongly affected by the properties of the sample material.

3.2.1. Structure

Top and side views of the suspended ring resonator concept are shown in Fig. 5.
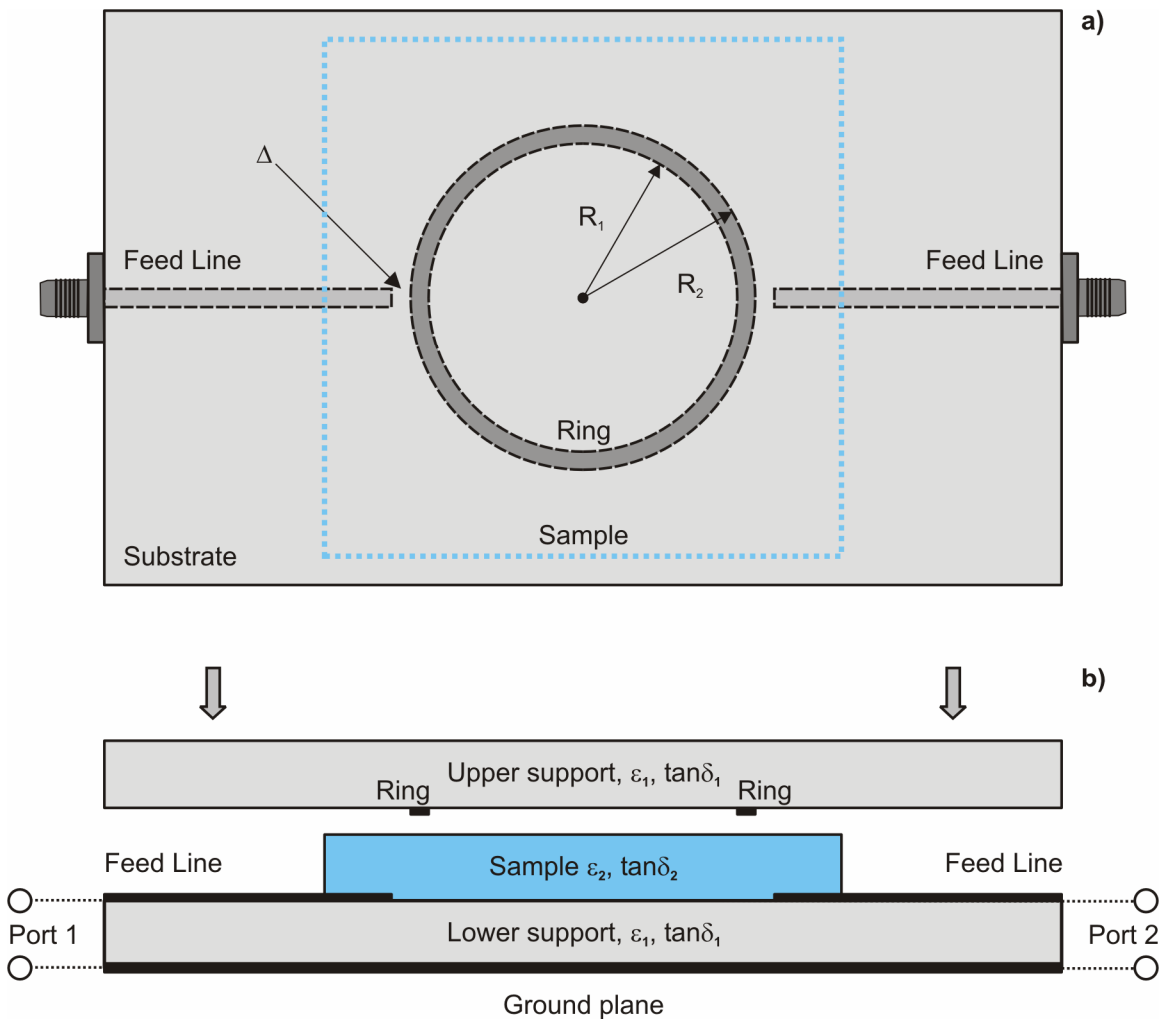
Fig. 5 Suspended ring resonator for measurement of arbitrary sample material shown from a) top and b) side views.

As shown above, the material to be measured is placed between two supports of known dielectric constant and loss tangent. The lower surface of the lower support is fully metallized to provide a ground plane for the feed lines and microstrip ring resonator. A small air gap is

included between the top surface of the sample and the microstrip ring to allow easy insertion and removal of the sample. The sample is larger than the ring to account for fringing fields around the microstrip ring; a square dimension of $1.5R_2$ is sufficient. The feed structure is similar to that of the planar resonator; two 50 Ω microstrip transmission lines are printed on the upper surface of the lower support and direct energy into and out of the ring resonator.

3.2.2. Network Parameter Formulation

The overall network parameter formulation of the suspended ring device is the same as that for the planar ring device. The schematics in Fig. 2, Fig. 3, and Fig. 4 apply directly to the suspended ring concept. As will be shown in the below sections, the primary difference between the analysis of the device in Fig. 1 and that in Fig. 5 is in the calculation of the propagation parameters for the microstrip ring.

3.2.3. Feed-Ring Interface

In the suspended ring design, the microstrip ring is in a different plane than that of the feed lines. I have chosen to consider the feed gap Δ as if the ring were projected onto the upper surface of the lower support. Though not an ideal model, this approximation captures the essence of the capacitive coupling in the sense that the fringing fields at the end of the feed line interact with the fringing fields of the microstrip ring. This interaction allows one feed line to excite fields in the ring and the other to sense fields in the ring.

3.2.4. Microstrip Ring Resonator

The microstrip ring resonator in Fig. 5 is largely similar to that in Fig. 1, with the exception that the suspended ring resonator has a multilayer dielectric substrate as well as a dielectric superstrate with a non-unity dielectric constant. The primary difference the analysis of these two structures is the calculation of the complex propagation constant γ and characteristic impedance

Z_0. While for the planar ring resonator I was able to apply simple microstrip theory to determine the propagation constant and characteristic impedance, the multilayer dielectric case is somewhat more complicated. In [42], Svačina develops a theory of multilayer dielectric microstrip transmission lines using a conformal mapping method. I have applied this theory to the problem of determining the propagation characteristics of the microstrip ring resonator in the suspended ring resonator device. The dielectric environment for the microstrip ring consists of five layers:

Table 1 Dielectric layers for suspended ring resonator.

Layer	Description
1	Lower support (ε_1, $\tan \delta_1$)
2	Sample (ε_2, $\tan \delta_2$)
3	Air gap (ε_{air}, $\tan \delta_{air}$)
4	Upper support (ε_1, $\tan \delta_1$)
5	Atmosphere (ε_{air}, $\tan \delta_{air}$)

Layers 1-3 are below the ring and layers 4 and 5 are above the ring. Each layer is assigned a filling factor based on the thickness of the layer as compared to the height of the microstrip above the ground plane and the width of the microstrip compared to its height over the ground plane. The filling factor of the ith layer is designated q_i, the width of the microstrip ring is designated W, the height of the microstrip ring above the ground plane is designated h, and the ratio of the height above the ground plane of the upper surface of the ith dielectric layer to h is designated H_i. For a wide ring, where W is greater than or equal to h:

$$q_1 = \frac{H_1}{2}\left[1 + \frac{\pi}{4} - \frac{h}{W_e}\ln\left(2\frac{W_e}{h}\frac{\sin\frac{\pi H_1}{2}}{H_1} + \cos\frac{\pi H_1}{2}\right)\right] \tag{33}$$

$$q_2 = \frac{H_2}{2}\left[1 + \frac{\pi}{4} - \frac{h}{W_e}\ln\left(2\frac{W_e}{h}\frac{\sin\frac{\pi H_2}{2}}{H_2} + \cos\frac{\pi H_2}{2}\right)\right] - q_1 \tag{34}$$

$$q_3 = 1 - \frac{h}{2W_e}\ln\left(\frac{\pi W_e}{h} - 1\right) - q_2 \tag{35}$$

$$q_4 = \frac{h}{2W_e}\left[\ln\left(\frac{\pi W_e}{h} - 1\right) - (1 + V_4)\ln\left(2\frac{W_e}{h}\frac{\cos\frac{\pi V_4}{2}}{2H_4 + V_4 - 1} + \sin\frac{\pi V_4}{2}\right)\right] \tag{36}$$

$$q_5 = 1 - \sum_{i=1}^{4} q_i \tag{37}$$

where

$$W_e = W + \frac{2h}{\pi}\ln\left[17.08\left(\frac{W}{2h} + 0.92\right)\right] \tag{38}$$

$$V_j = \frac{2}{\pi}\arctan\left[\frac{\pi}{\frac{\pi W_e}{2h} - 2}(H_j - 1)\right] \tag{39}$$

For a narrow ring with W less than h, the following filling factors are used:

$$q_1 = \frac{\ln A_1}{2\ln\frac{8h}{W}}\left(1 + \frac{\pi}{4} - \frac{1}{2}\arccos\frac{W\sqrt{A_1}}{8hH_1}\right) \tag{40}$$

$$q_2 = \frac{\ln A_2}{2\ln\frac{8h}{W}}\left(1 + \frac{\pi}{4} - \frac{1}{2}\arccos\frac{W\sqrt{A_2}}{8hH_2}\right) - q_1 \tag{41}$$

$$q_3 = \frac{1}{2} + \frac{0.9}{\pi\ln\frac{8h}{W}} - q_2 \tag{42}$$

24

$$q_4 = \frac{1}{2} - \frac{0.9 + \frac{\pi}{4}\ln B_4 \arccos\left[\left(1 - \frac{1 - \frac{W}{8h}}{H_4}\right)\sqrt{B_4}\right]}{\pi \ln \frac{8h}{W}} \tag{43}$$

$$q_5 = 1 - \sum_{i=1}^{4} q_i \tag{44}$$

where

$$A_i = \frac{1 + H_i}{1 - H_i + \frac{W}{4h}}, \quad B_j = \frac{H_j + 1}{H_j + \frac{W}{4h} - 1} \tag{45}$$

The effective dielectric constant of the multilayer microstrip ring is calculated from the dielectric constant of each layer material and the filling factors:

$$\varepsilon_e = \frac{\left(\sum_{i=1}^{3} q_i\right)^2}{\sum_{i=1}^{3} \frac{q_i}{\varepsilon_i}} + \frac{\left(\sum_{j=4}^{5} q_j\right)^2}{\sum_{j=4}^{5} \frac{q_j}{\varepsilon_j}} \tag{46}$$

where ε_i is the complex dielectric constant of the ith layer and ε_j is the complex dielectric constant of the jth layer. The propagation constant γ is then

$$\gamma = j\omega\sqrt{\mu_0 \varepsilon_0 \varepsilon_e} \tag{47}$$

It is important to note the relationship in (46) between the dielectric constant of the microstrip mode ε_e and the individual layer dielectric constants ε_i; the terms of ε_e vary as the reciprocal of the sum of the reciprocals of the ε_i. This means that ε_e is dominated by low dielectric constant layers, such as the air gap above the sample. A close analogy is given by a parallel resistor circuit where individual resistances play similar roles to the ε_i. A consequence of this is that

high dielectric constant samples will be measured less accurately by this device. Low dielectric constant samples, such as EPS foam, will be accurately measured.

For thick samples, the height of the microstrip ring resonator above the ground plane may be relatively large compared to the width of the microstrip and the guided wavelength of waves at the resonant frequencies. As a result, the ring may exhibit relatively significant radiation losses that will affect the frequency and bandwidth of the ring resonances. In order to take this radiation into account, I use semi-analytical techniques presented by Hill, Camell, Cavcey, and Koepke [44]. They develop methods for calculating the electric far-field of a straight length of microstrip. To apply this model, the microstrip ring can again be modeled as two parallel microstrips due to its low curvature [39]. The authors of [44] first calculate the so-called array factor A_L for the microstrip:

$$A_L = \frac{\sin\left[(k_e - k\sin\theta\cos\phi)\dfrac{L}{2}\right]}{(k_e - k\sin\theta\cos\phi)\dfrac{L}{2}} \tag{48}$$

where k is the free-space wavenumber, k_e is the microstrip mode of the wavenumber, L is the length of the microstrip, and (θ, ϕ) are spherical coordinates centered on the microstrip:

$$k = \omega\sqrt{\mu_0\varepsilon_0} \tag{49}$$

$$k_e = k\sqrt{\varepsilon_e} \tag{50}$$

The array factor does not have a meaning of the real array factor for an array of the sources; it's introduction here is only a matter of convenience. Two other supplementary quantities are then calculated:

$$R_v = \frac{1 - \dfrac{jv\tan(kvh)}{\varepsilon_{sr}\cos\theta}}{1 + \dfrac{jv\tan(kvh)}{\varepsilon_{sr}\cos\theta}} \tag{51}$$

$$R_h = \frac{1 + \dfrac{jv\cot(kvh)}{\cos\theta}}{1 - \dfrac{jv\cot(kvh)}{\cos\theta}} \tag{52}$$

where v is dependent on ε_{sr} and h is the height of the microstrip above the ground plane:

$$v = \sqrt{\varepsilon_{sr} - 1} \tag{53}$$

$$\varepsilon_{sr} = \sum_{i=1}^{4} \varepsilon_i \frac{t_i}{h} \tag{54}$$

where ε_i and t_i are the real dielectric constant and thickness of the ith dielectric layer above the ground plane. Then, the authors calculate the electric field in θ- and ϕ-planes due to the currents flowing along the microstrip:

$$E_{\theta h} = \frac{j\omega\mu_0 I_0 LA_L}{4\pi}(R_v - 1)\cos\theta\cos\phi\frac{e^{-jkr}}{r} \tag{55}$$

$$E_{\phi h} = \frac{j\omega\mu_0 I_0 LA_L}{4\pi}(R_h + 1)\sin\phi\frac{e^{-jkr}}{r} \tag{56}$$

where r is the distance from the origin in spherical coordinates. To account for radiation from the vertical currents at the feed points of the ring, a third supplementary quantity might be needed:

$$F = j2\sin\left[(k_e - k\sin\theta\cos\phi)\frac{L}{2}\right] \tag{57}$$

$$E_{\theta v} = \frac{1}{2}\frac{j\omega\mu_0 I_0 F}{4\pi\varepsilon_{sr}kv}(R_v + 1)\tan(kvh)\sin\theta\frac{e^{-jkr}}{r} \tag{58}$$

The factor of one-half is added to account the vertical currents are shared between the two halves of the microstrip ring resonator. The vertical currents at the feed points do not contribute to the

electric field in the ϕ-plane [44]. The radiation efficiency of the microstrip, E_{rad}, is calculated as the quotient of the power radiated over a sphere of radius r and incident power:

$$E_{rad} = \frac{P_{rad}}{P_{inc}} \tag{59}$$

$$P_{rad} = r^2 \int_0^{2\pi} \int_0^{\pi/2} \frac{|E_\theta|^2 + |E_\phi|^2}{\eta} \sin\theta\, d\theta\, d\phi \tag{60}$$

$$P_{inc} = |I_0|^2 Z_0 \tag{61}$$

The squared magnitude of the unknown initial current I_0 appears in the numerator of P_{rad} and P_{inc} and cancels, leaving E_{rad} independent of applied power.

I include the additional loss due to radiation as an additional real term in the expression for the propagation constant γ. The fraction of applied power that reaches the end of a microstrip is reduced by the radiation efficiency of the microstrip. The power lost per unit length is then

$$P_{lost} = \frac{P_{inc} E_{rad}}{L} \tag{62}$$

The S_{21} parameter of a matched microstrip line of length L takes the form

$$S_{21} = e^{-\gamma L} \tag{63}$$

Adding a real term to γ is equivalent to modifying the S_{21} parameter expression by including an exponential factor:

$$S_{21} = e^{-(\gamma+R)L} = e^{-\gamma L} e^{-RL} \tag{64}$$

The term R can be found from the application of perturbation theory to a lossy transmission line as detailed on page 83 of [45]:

$$R = \frac{P_{lost}}{2 P_{inc}} = \frac{E_{rad}}{2L} \tag{65}$$

and the propagation constant including radiation effects is

$$\gamma_{\text{rad}} = \gamma + R \tag{66}$$

For the suspended ring resonator, γ_{rad} replaces γ in the S-parameters describing the microstrip ring. The MATLAB file `RingRadiation.m` calculates the radiation efficiency and is called by `RingSandwich.m`.

3.2.5. Complete Device Model

As for the planar ring resonator device, the overall response of the suspended ring resonator shown in Fig. 5 is calculated as the product of the ABCD parameter formulations of the left feed gap, the microstrip ring, and the right feed gap. Once again, the S_{21} scattering parameter is calculated from the ABCD parameter formulation of the suspended ring resonator:

$$S_{21} = \frac{2}{A + \dfrac{B}{Z_0} + Z_0 C + D} \tag{67}$$

$$S_{21} = \frac{8 Z_0 Z_{ring} C_g^2 e^{-\gamma_{\text{rad}} L} \omega^2}{\Psi}$$

$$
\begin{aligned}
\Psi = {} & 4\left(e^{-2\gamma_{\text{rad}} L} - 1\right) \\
& + j4\omega \left(\begin{array}{l} 2Z_0 C_p e^{-2\gamma_{\text{rad}} L} + 2Z_0 C_g e^{-2\gamma_{\text{rad}} L} - Z_{ring} C_g e^{-2\gamma_{\text{rad}} L} \\ - Z_{ring} C_g - 2Z_0 C_g - 2Z_o C_p \end{array} \right) \\
& + \omega^2 \left(\begin{array}{l} 4Z_0^2 C_p^2 + 8Z_0^2 C_g C_p + Z_{ring}^2 C_g^2 + 8Z_0 Z_{ring} C_g C_p + 4Z_0^2 C_g^2 + 4Z_0 Z_{ring} C_g^2 \\ - 8Z_0^2 C_g C_p e^{-2\gamma_{\text{rad}} L} + 8Z_0 Z_{ring} C_g C_p e^{-2\gamma_{\text{rad}} L} + 4Z_0 Z_{ring} C_g^2 e^{-2\gamma_{\text{rad}} L} \\ - 4Z_0^2 C_g^2 e^{-2\gamma_{\text{rad}} L} - 4Z_0^2 C_p^2 e^{-2\gamma_{\text{rad}} L} - Z_{ring}^2 C_g^2 e^{-2\gamma_{\text{rad}} L} \end{array} \right) \\
& + j2\omega^3 \left(\begin{array}{l} 2Z_0 Z_{ring} C_g^2 C_p + 2Z_0^2 Z_{ring} C_g C_p^2 + Z_0 Z_{ring}^2 C_g^2 C_p + 2Z_0^2 Z_{ring} C_g C_p^2 e^{-2\gamma_{\text{rad}} L} \\ + 2Z_0^2 Z_{ring} C_g^2 C_p e^{-2\gamma_{\text{rad}} L} - Z_0 Z_{ring}^2 C_g^2 C_p e^{-2\gamma_{\text{rad}} L} \end{array} \right) \\
& + \omega^4 Z_0^2 Z_{ring}^2 C_g^2 C_p^2 \left(e^{-2\gamma_{\text{rad}} L} - 1\right)
\end{aligned}
\tag{68}
$$

where Z_0 is the characteristic impedance of the measurement system and feed lines, Z_{ring} is the characteristic impedance of the microstrip ring resonator, and L is πR_m. Z_0 is calculated from the formulas in [40] and [41] and Z_{ring} is calculated from formulas in [43]:

$$Z_{ring} = \frac{120\pi}{\sqrt{\varepsilon_e}} \frac{\text{h}}{\text{W}_\text{e}}, \frac{W}{h} \geq 1 \tag{69}$$

$$Z_{ring} = \frac{60}{\sqrt{\varepsilon_e}} \ln \frac{8h}{W}, \frac{W}{h} < 1 \tag{70}$$

3.3. Raw Measurement Processing

The theory leading to an expression for the S_{21} parameter of the ring resonator device shown in Fig. 5 can be applied to find unknown dielectric constants and loss tangents. In particular, the location and bandwidth of peaks in a plot of the S_{21} parameter versus frequency will vary with the dielectric constant and loss tangent of the material in the sample layer. Table 2 contains the details of the layer stack-up for simulation of a fictitious sample material with a dielectric constant between one and ten. Using the theory from the above sections, the variation in the frequency of the first resonance of a suspended ring resonator can be calculated. For this simulation, the ring and feed lines had a width of 2.2 mm and the ring mean radius was 25.9 mm. The simulation was performed for sample ε_r from one to ten at intervals of 0.1, and the results are shown in Fig. 6 for the frequency of the first resonance and Fig. 7 for the frequency of the second resonance. Table 3 contains the layer stack-up information for the simulation of a fictitious sample material with a dielectric constant of 4 and a loss tangent between 0 and 0.05. The variation of loaded quality (Q) factor with loss tangent for the first two resonances is shown in Fig. 8 and Fig. 9. Loaded Q factors are calculated for each resonance as

$$Q_{\text{loaded}} = \frac{f_{\text{res}}}{f_{\text{3dB,U}} - f_{\text{3dB,L}}} \tag{71}$$

where f_{res} is the resonant frequency and $f_{\text{3dB,U}}$ and $f_{\text{3dB,L}}$ are the upper and lower half-power frequencies, respectively; f_{res}, $f_{\text{3dB,U}}$, and $f_{\text{3dB,L}}$ are found from the S_{21} scattering parameter for the ring resonator.

The resonance locations and bandwidths are calculated using `RingSandwich.m`, which can be found in Appendix A along with supporting function m-files `microstrip.m`, `microstrip_nlayer.m`, and `gap_capacitance.m`. In the sections below, I will present further results verifying the use of this theory for the determination of dielectric constants.

Table 2 Layer detail for variable ε_r material example.

Layer	Description	Material	Thickness [mm]	ε_r	tanδ
1	Lower support (ε_1, tan δ_1)	FR-4	1.575	4.25	0.016
2	Sample (ε_2, tan δ_2)		5	1-10	0
3	Air gap (ε_{air}, tan δ_{air})	Air	0.5	1.00059	0
4	Upper support (ε_1, tan δ_1)	FR-4	1.575	4.25	0.016
5	Atmosphere (ε_{air}, tan δ_{air})	Air		1.00059	0

Table 3 Layer detail for variable tanδ material example.

Layer	Description	Material	Thickness [mm]	ε_r	tanδ
1	Lower support (ε_1, tan δ_1)	FR-4	1.575	4.25	0.016
2	Sample (ε_2, tan δ_2)		5	4	0-0.05
3	Air gap (ε_{air}, tan δ_{air})	Air	0.5	1.00059	0
4	Upper support (ε_1, tan δ_1)	FR-4	1.575	4.25	0.016
5	Atmosphere (ε_{air}, tan δ_{air})	Air		1.00059	0

Fig. 6 Variation of $f_{res,1}$ vs. ε_r of a 5 mm thick sample.
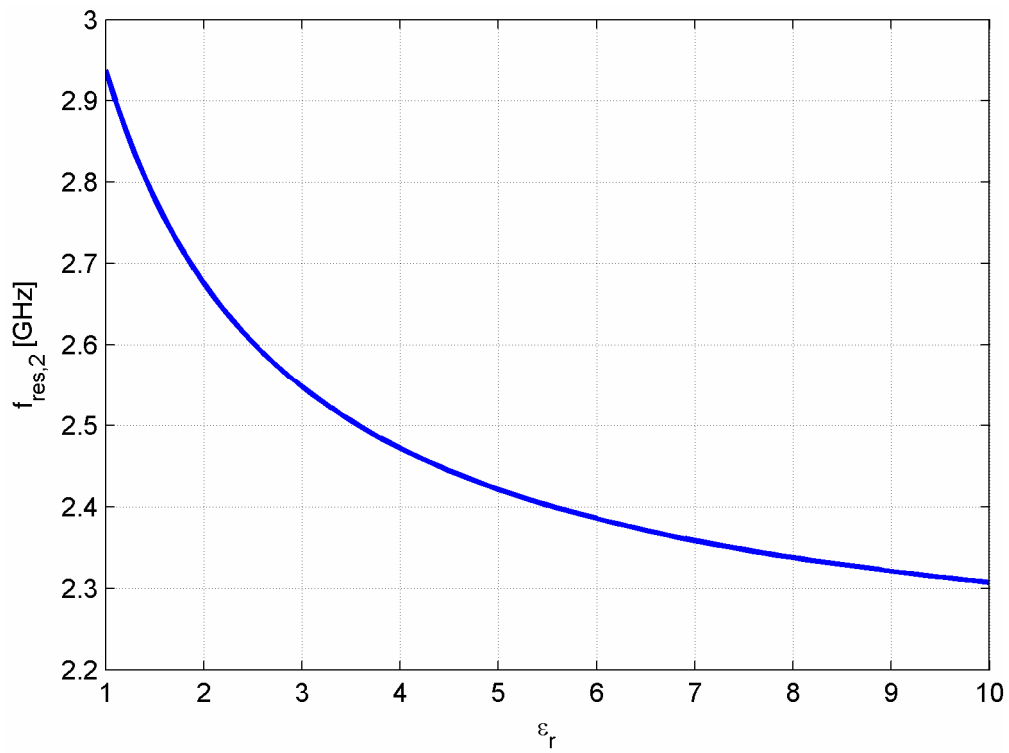
Fig. 7 Variation of $f_{res,2}$ vs. ε_r of a 5 mm thick sample.
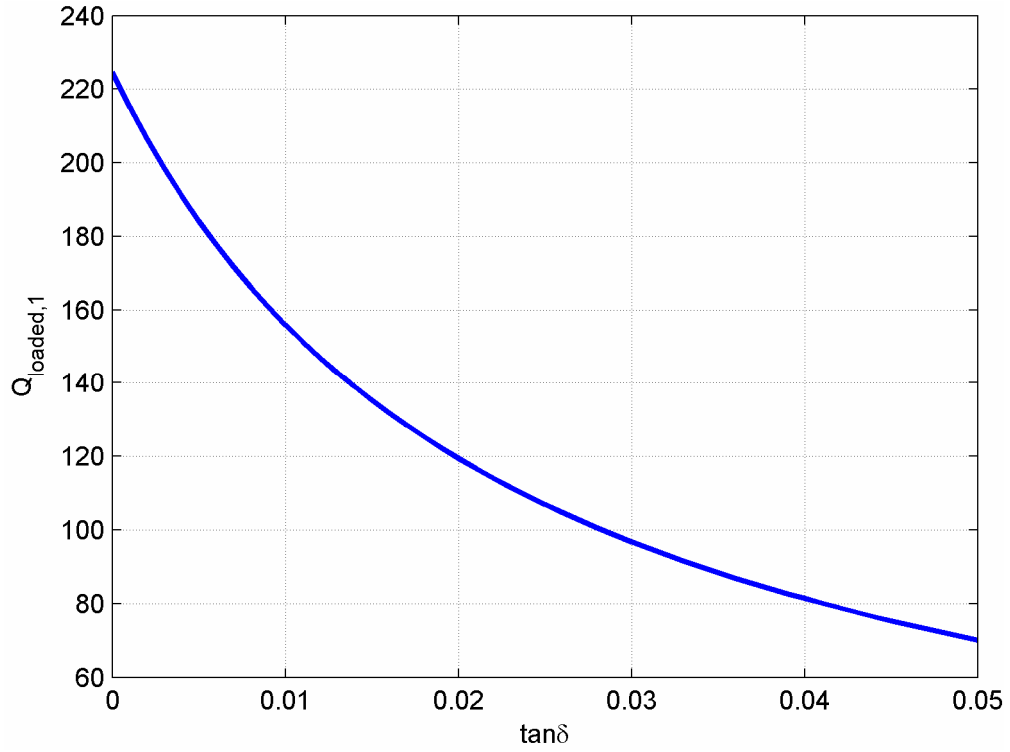
Fig. 8 Variation of $Q_{loaded,1}$ vs. tanδ of a 5 mm sample.
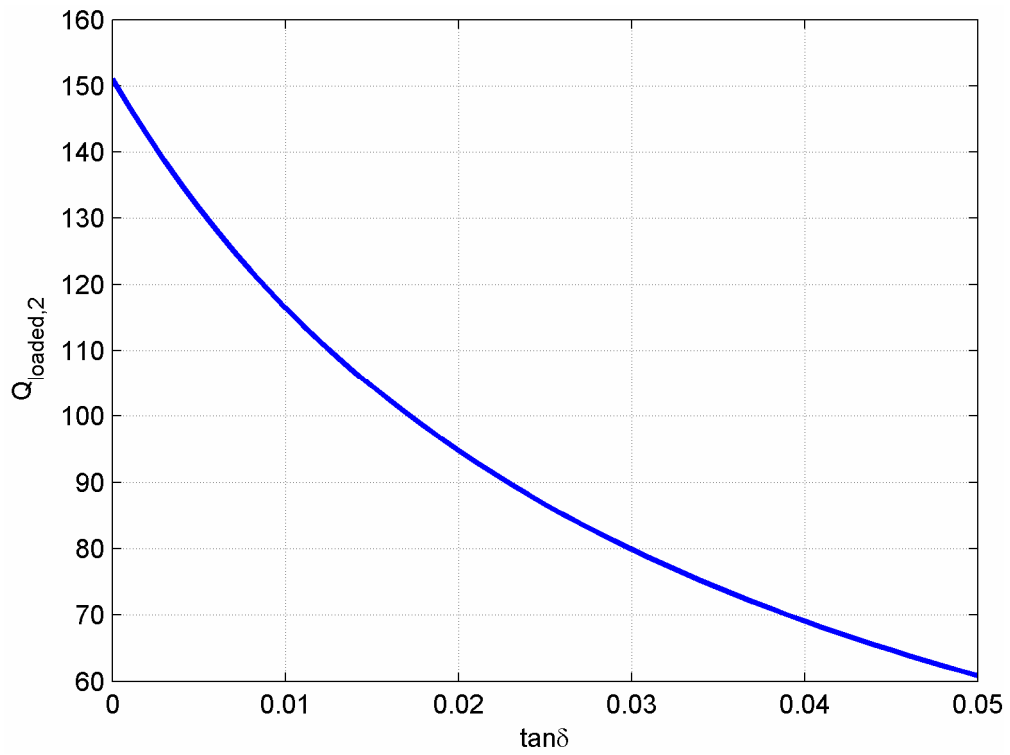
Fig. 9 Variation of $Q_{loaded,2}$ vs. tand of a 5 mm sample.

4. Experimental Verification

In this section I present descriptions of test setups for the planar and suspended ring resonator concepts as well as dielectric measurement results obtained with both types of resonator. Unless otherwise noted, all measurements were taken at room temperature using a HP/Agilent 8722ET network analyzer.

4.1. Planar Ring Resonator Test Setup

I designed and constructed a planar ring resonator similar to Fig. 1 in order to verify the network parameter theory could be used to determine the dielectric constant and loss tangent of a known substrate. Fig. 10 is a photograph of the constructed device.
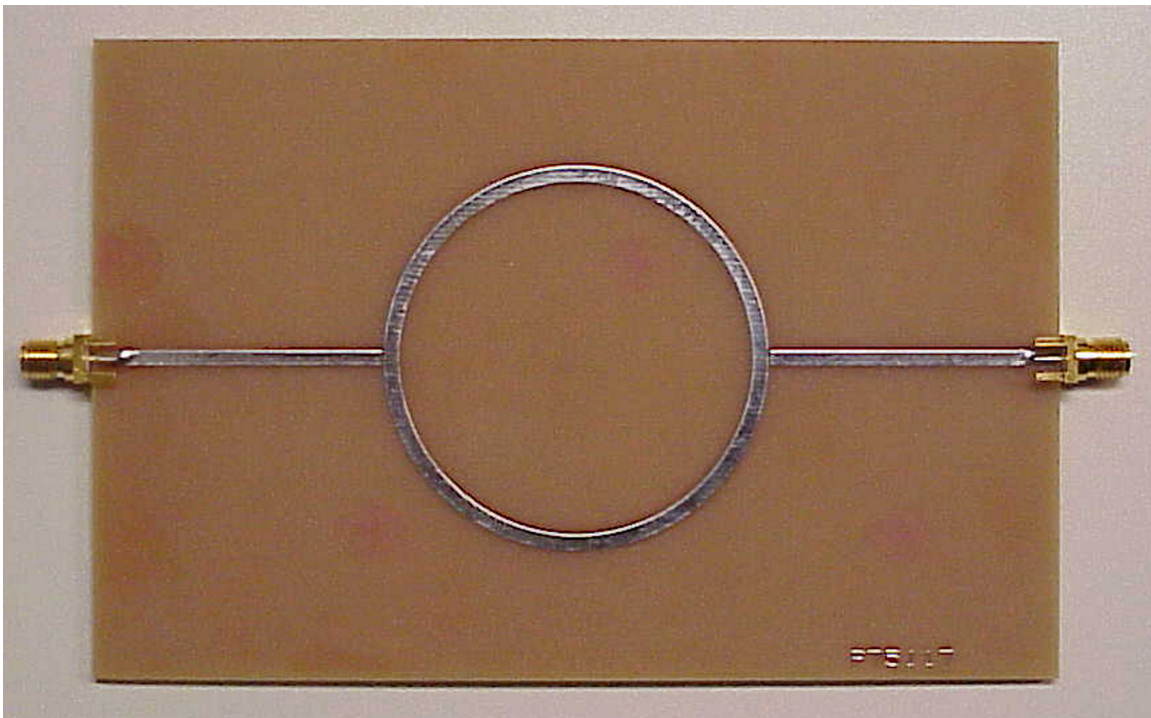
Fig. 10 Constructed planar ring resonator.

4.1.1. Structural Details

The ring and feed lines are 2.2 mm wide, and the ring resonator has a mean radius of 25.9 mm. The gap between each feed line and the ring is 0.25 mm. The substrate is 62 mil thick FR-4 manufactured by Isola Laminate Systems Corp.; an Isola datasheet lists the dielectric constant

and loss tangent of this material as 4.25 and 0.016 at 1 GHz. The dimensions of the substrate are 136x90 mm, and the bottom surface of the substrate is fully metallized. SMA connectors enable attachment to measuring equipment. The board was printed and etched by Advanced Circuits, Inc., of Aurora, CO. I performed final assembly and soldering at WPI.

4.1.2. Simulation Results

The device shown in Fig. 10 was connected to a network analyzer and subjected to a frequency sweep from 800 MHz to 2.4 GHz at intervals of 1 MHz. The magnitude of the S_{21} parameter was recorded at each frequency point. I simulated the S_{21} response of the planar ring resonator at the same frequency points. The microstrip and gap capacitance parameters were calculated according to the formulas presented in section 3.1, above, and are listed in Table 4. Performance values for the first two resonances are listed in Table 5, and simulated and measured S_{21} parameters for this device are shown in Fig. 11. As the authors of previous works [21]-[23], the simulated S_{21} parameter matches well with the measured data, validating the use of network parameter formulations for the simulation of planar ring resonators.

Table 4 Planar ring resonator parameters.

Parameter	Value	Units
ε_e	3.103	
Z_0	61.34	Ω
C_p	9.266	fF
C_g	82.90	fF

Table 5 Planar ring resonator performance.

	Measured Value	Simulated Value	Units
$f_{res,1}$	1.034	1.035	GHz
$f_{res,2}$	2.068	2.070	GHz
$BW_{res,1}$	22	22	MHz
$BW_{res,2}$	40	44	MHz
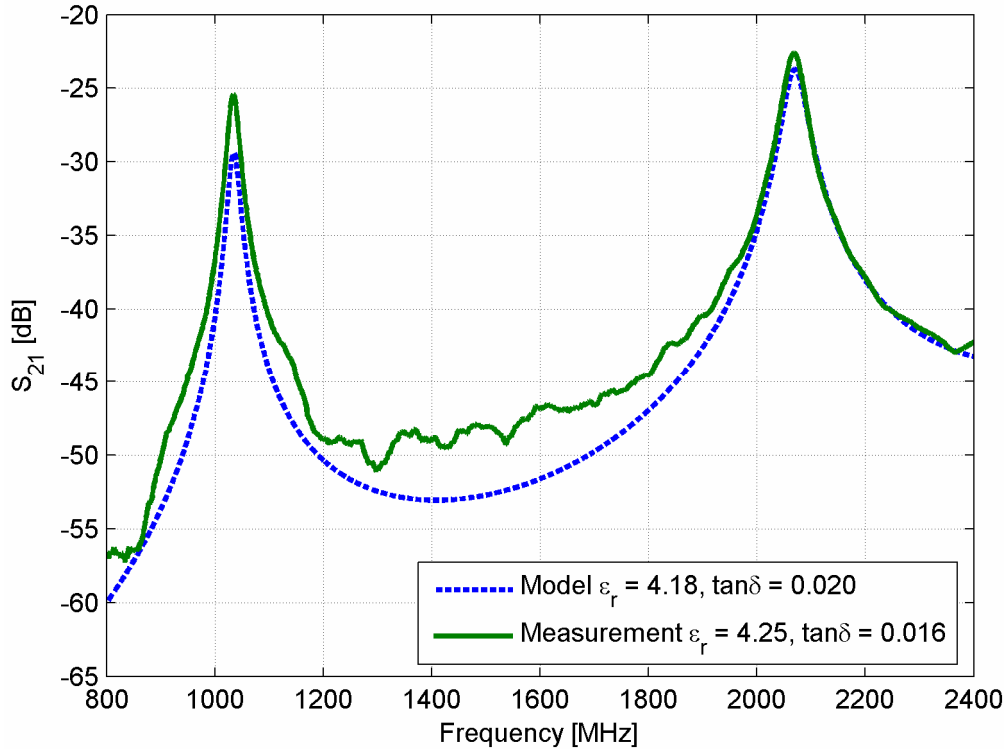
Fig. 11 S_{21} parameter of planar ring resonator.

4.2. Suspended Ring Resonator Test Setup

In order to verify the suspended ring resonator concept, I designed and constructed the device in Fig. 12. This device was used to determine the dielectric constant and loss tangent of expanded polystyrene (EPS) foam samples.

4.2.1. Structural Details

The upper and lower supports are 62 mil thick FR-4 laminate from Isola Laminate Systems Corp. The supports are mounted using metric positioning equipment from Edmund Industrial Optics, Inc. The lower support attaches to a laboratory jack, part number NT54-687; the top board mounts independently in a fixed position using two two-part posts, part numbers NT54-939/956. The jack and posts attach directly to a bench plate, part number NT54-638. As with the planar ring resonator, the feed lines and microstrip ring are 2.2 mm wide, and the lower

surface of the lower support is fully metallized. In Fig. 12, a sample of EPS foam is shown underneath the ring; this sample is smaller than the actual samples measured. The laboratory jack is used to assign the vertical position of the sample with respect to the ring on the lower surface of the upper support. The four long screws that mount the upper support also provide support for a copper shield to partially protect the resonator from the room's EM environment.
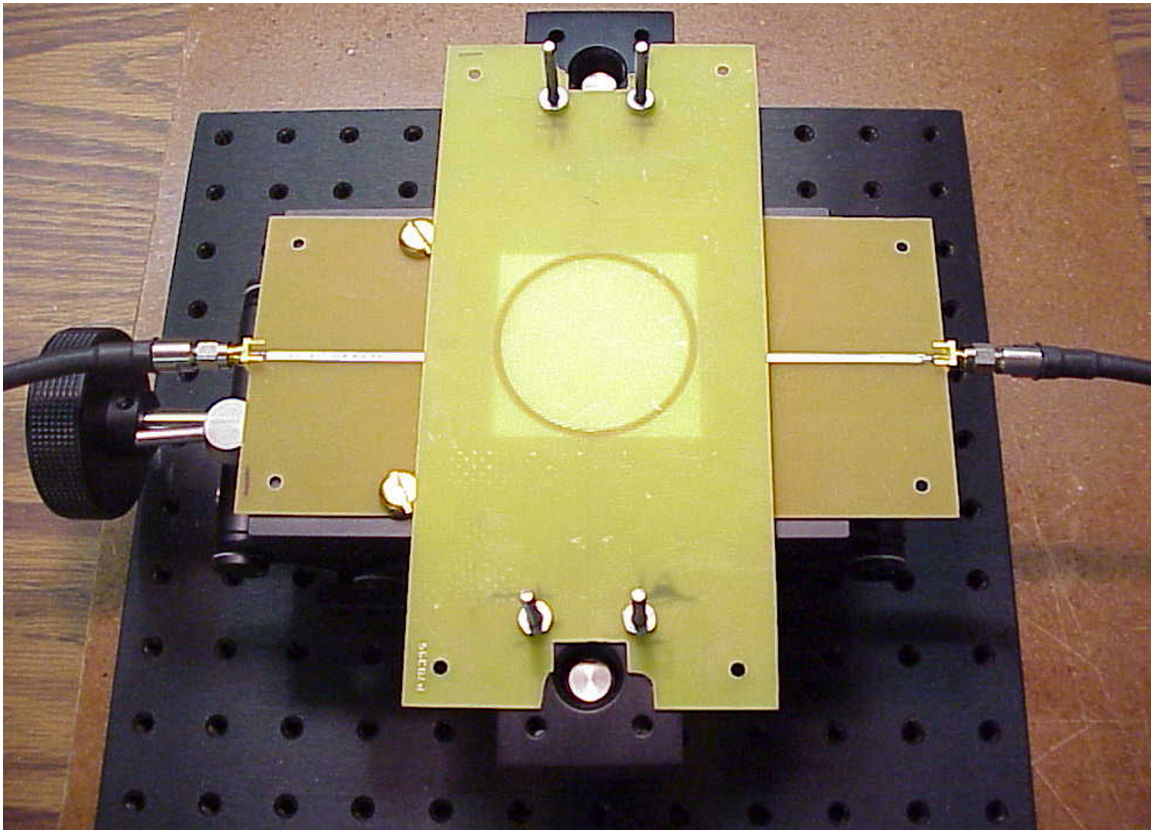
Fig. 12 Constructed suspended ring resonator.

4.2.2. Simulation Results

Using MATLAB, I simulated the suspended ring resonator in Fig. 12 to determine the relationship between sample ε_r and the shift in the first and second resonances. For this exercise, I assumed 6.22 mm thick sample with 0.75 mm air gap. Both resonances exhibit nearly linear dependence on the sample dielectric constant, as shown in Fig. 13 for the first resonance and Fig. 14 for the second resonance. I fit, in a least-squares sense, a 3rd-order polynomial to the data for

each resonance. This results in a maximum error, over the simulated dielectric constants, of 3.9

x 10^{-7} in ε_r for the first resonance and 3.1 x 10^{-7} in ε_r for the second resonance.
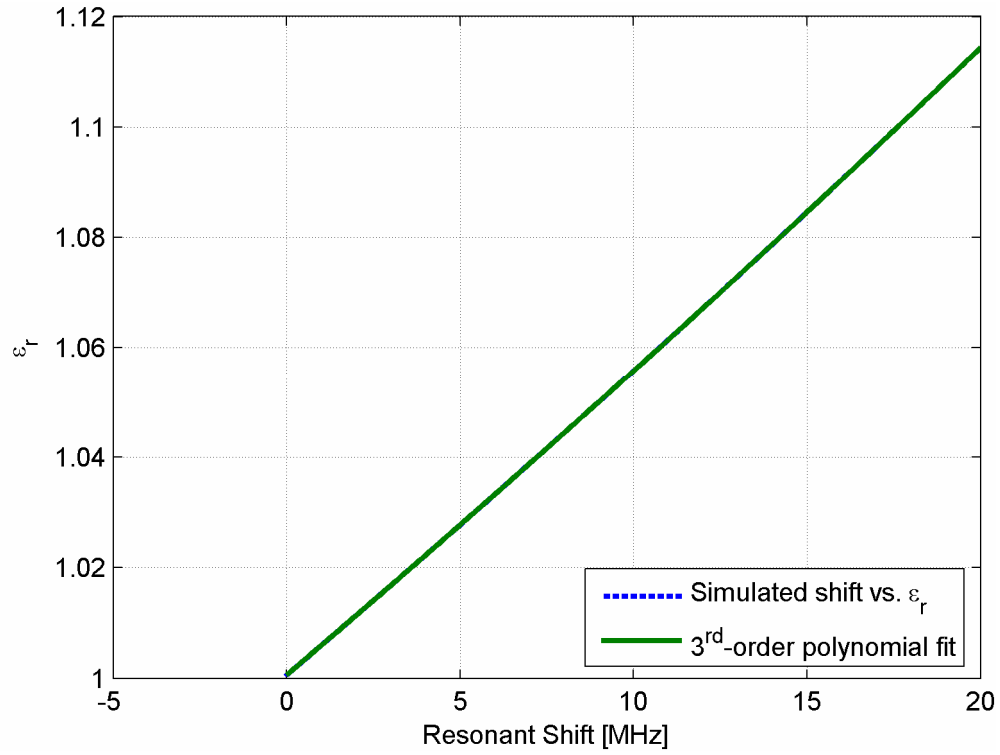
Fig. 13 ε_r vs. shift in first resonance for 6.22 mm sample with 0.75 mm air gap.
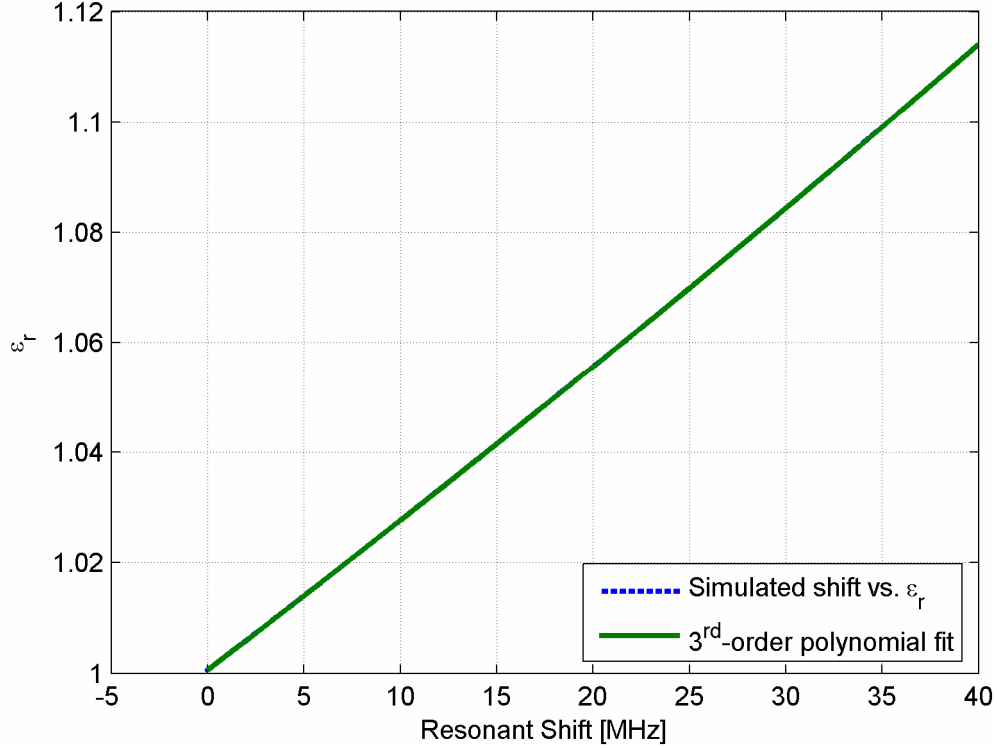
Fig. 14 ε_r vs. shift in second resonance for 6.22 mm sample with 0.75 mm air gap.

Table 6 lists the coefficients of the polynomials in the form:

$$\varepsilon_r = a_3 f_\Delta^3 + a_2 f_\Delta^2 + a_1 f_\Delta + a_0 \qquad (72)$$

where f_Δ is the resonant frequency shift. The MATLAB file `MultiErFoam.m` can be found in Appendix A.

Table 6 3rd-order polynomials for suspended ring resonator resonance shift vs. ε_r.

Resonance	a_3	a_2	a_1	a_0
1	5.282E-08	1.596E-05	5.348E-03	1.001
2	6.556E-09	3.975E-06	2.667E-03	1.001

Given the frequency shift in the first and second resonances, the polynomial coefficients in Table 6 can predict the dielectric constant of a 6.22 mm (245 mil) thick sample material at the resonances. Fig. 15 shows measurement results for the first resonance of the suspended ring resonator when loaded with a 6.22 mm thick foam sample with density 21.6 kg/m^3; Fig. 16 shows measurement results for the second resonance of the suspended ring resonator with the

39

same sample. Measurements of S_{21} were made over a band of 40 MHz with 1601 frequency points, vertical resolution of 5dB/div, and reference -30 dB. The sweep time was manually set to 5 sec and the averaging and smoothing options of the network analyzer were disabled. The peak magnitude of S_{21} corresponding to a resonance was recorded at intervals of 5 sec using automatic marker tracking.

Fig. 15 and Fig. 16 also contain plots of two estimates for foam dielectric constant. The dashed horizontal lines are Knott's prediction of foam dielectric constant, reported in [2]

$$\varepsilon_{\text{foam}} = \varepsilon_{\text{pol}}\left[1 - \frac{\left(\varepsilon_{\text{pol}} - \varepsilon_{\text{gas}}\right)\left(1 - \alpha\right)}{\varepsilon_{\text{gas}} + \left(\varepsilon_{\text{pol}} - \varepsilon_{\text{gas}}\right)^{1/3}}\right] \tag{73}$$

where ε_{pol} is the dielectric constant of the base polymer, ε_{gas} is the dielectric constant of the blowing agent gas, and α is the volumetric fraction of polymer in the foam:

$$\alpha = \frac{\rho_{\text{foam}}}{\rho_{\text{pol}}} \tag{74}$$

where ρ_{foam} and ρ_{pol} are the densities of the foam and base polymer. In [2], Knott cites a previous result by Cuming:

$$\ln \varepsilon_{\text{foam}} = \sum_i \alpha_i \ln \varepsilon_i \tag{75}$$

where α_i and ε_i are the volumetric fraction and dielectric constant of the ith component of the foamed mixture; this prediction is shown in Fig. 15 and Fig. 16 as the solid horizontal lines. Berrie and Wilson, using a slotted waveguide technique, confirmed Knott's formula (73) for EPS foam of density from 13 kg/m^3 to 29 kg/m^3 in [3]. Fig. 15 shows excellent agreement at the first resonance of my predictions of dielectric constant with Knott's formula. The second resonance results shown in Fig. 16 are slightly lower than those for the first resonance but generally still fall between the predictions by Cuming and Knott.
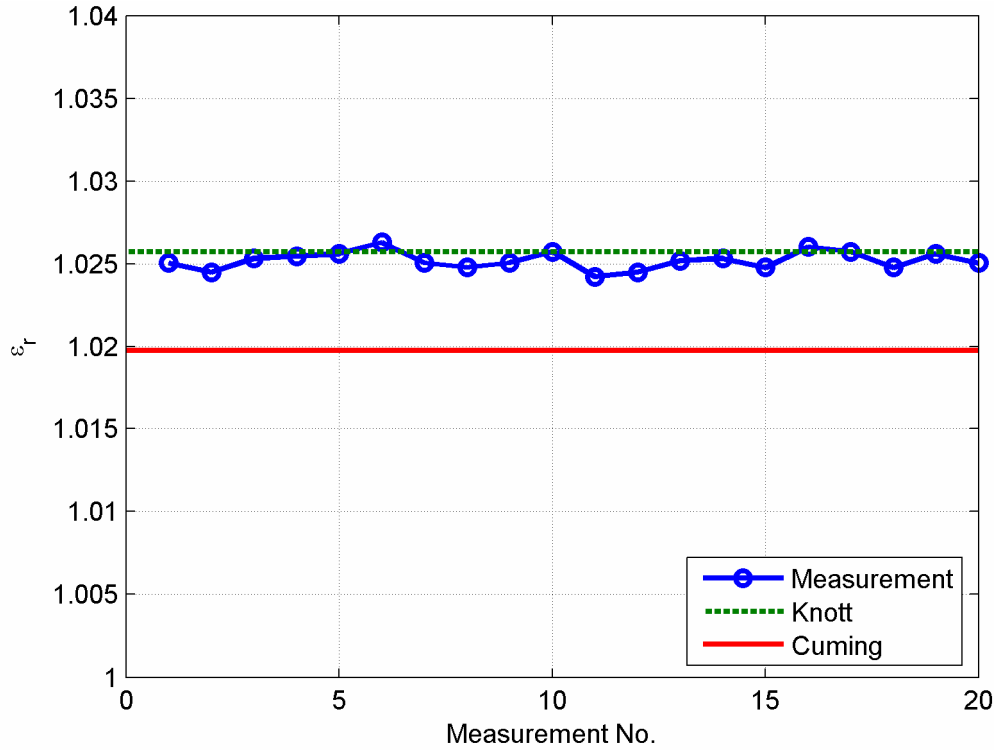
Fig. 15 Measured first resonance dielectric constants for 6.22 mm thick EPS foam.
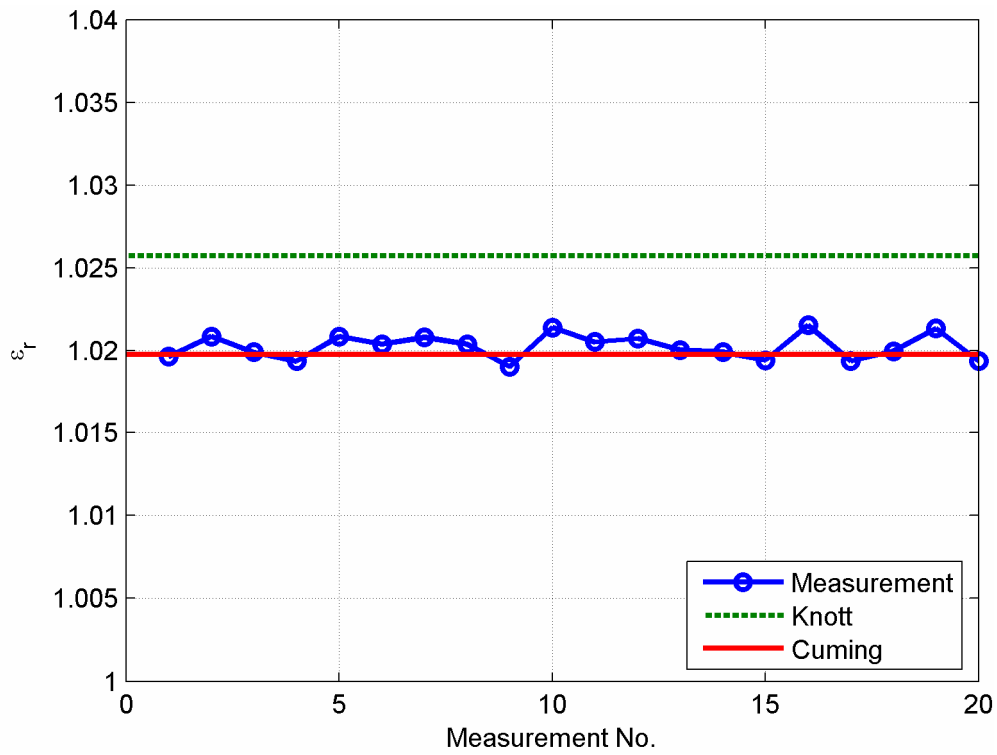
Fig. 16 Measured second resonance dielectric constants for 6.22 mm thick EPS foam.

Using the measured dielectric constant for the foam sample above, I simulated the suspended ring resonator to determine the relationship between a shift in loaded Q factor and the loss tangent for the first two resonances. Again, I calculated 3rd-order polynomials to approximate the simulation results. As for the dielectric constant, the simulations exhibit a mostly linear dependence of tanδ on the shift in Q factor. Results for the first resonance are shown in Fig. 17 and results for the second resonance are shown in Fig. 18. The maximum errors over the simulated values of loss tangent are 5.2 x 10^{-7} for the first resonance and 1.7 x 10^{-7} for the second resonance.
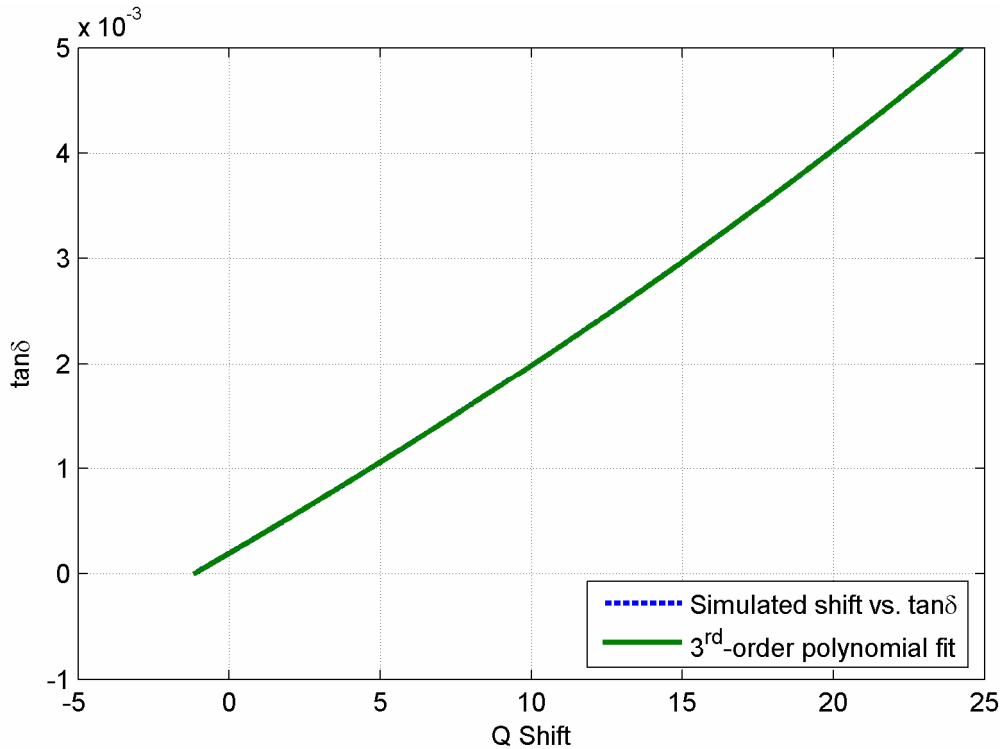
Fig. 17 tanδ vs. shift in first resonance Q factor for 6.22 mm sample with 0.75 mm air gap.
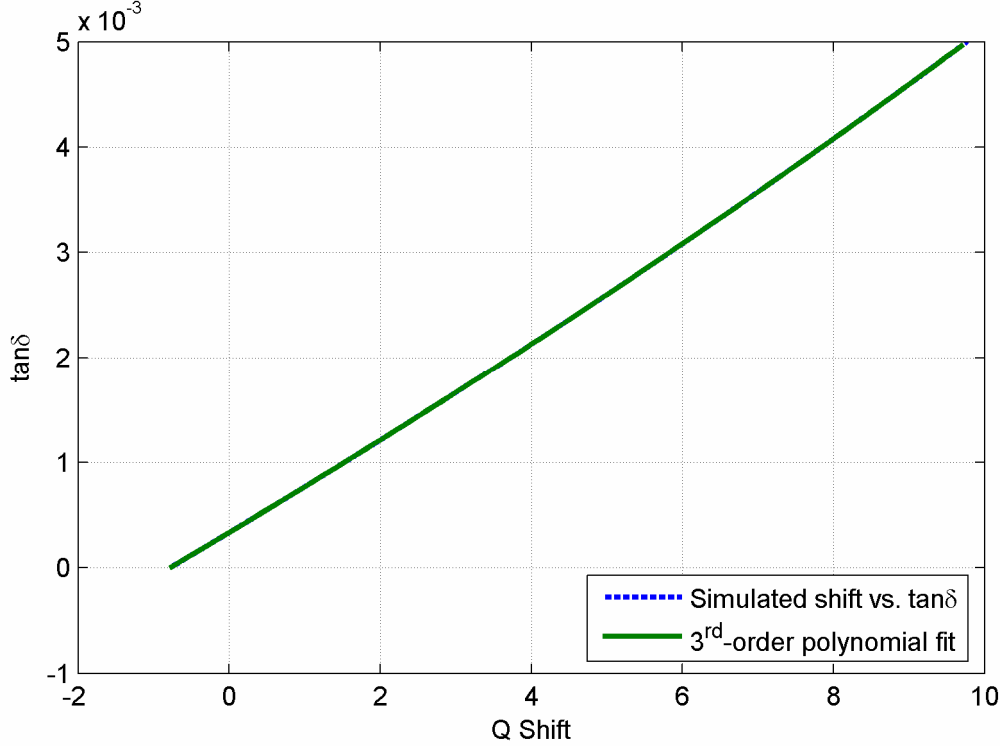
Fig. 18 tanδ vs. shift in second resonance Q factor for 6.22 mm sample with 0.75 mm air gap.

Table 7 shows the coefficients of the polynomials in the form

$$\tan \delta = a_3 Q_\Delta^3 + a_2 Q_\Delta^2 + a_1 Q_\Delta + a_0 \tag{76}$$

where Q_Δ is the shift in Q factor. The MATLAB file `MultiTanFoam.m` is included in Appendix A.

Table 7 3rd-order polynomials for suspended ring resonator Q factor shift vs. tanδ.

Resonance	a_3	a_2	a_1	a_0
1	9.743E-09	1.042E-06	1.672E-04	1.939E-04
2	5.668E-08	4.413E-06	4.292E-04	3.336E-04

Given the shift in Q factor between the air-filled resonator and the sample-filled resonator, the polynomial coefficients in Table 7 can be used to predict the loss tangent of a 6.22 mm (245 mil) thick sample material at the resonances. Fig. 19 shows measurement results for the first resonance of the suspended ring resonator when loaded with a 6.22 mm thick foam sample with density 21.6 kg/m^3; the results for the second resonance are shown in Fig. 20. Measurements of

S_{21} were made over a band of 20 MHz for the first resonance and 40 MHz for the second resonance with 1601 frequency points, vertical resolution of 1dB/div, and reference -30 dB. The sweep time was manually set to 5 sec and the averaging and smoothing options of the network analyzer were disabled. The Q factor, which is automatically calculated by the network analyzer, corresponding to a resonance was recorded at intervals of 5 sec using automatic marker tracking. For these measurements, a shield consisting of solid copper is placed above the ring resonator. This shield serves to reduce radiation losses dramatically and allows comparison of measurements with simulations that do not include radiation losses.

Fig. 19 and Fig. 20 also include lines indicating the loss tangent of bulk polystyrene. The results for the first resonance match very well with the loss tangent of the bulk material. However, the second resonance loss tangent measurements are much higher. This is likely due to radiation at the second resonance that is not taken into account; it is unlikely that the loss tangent undergoes such a dramatic increase between the first two resonances.
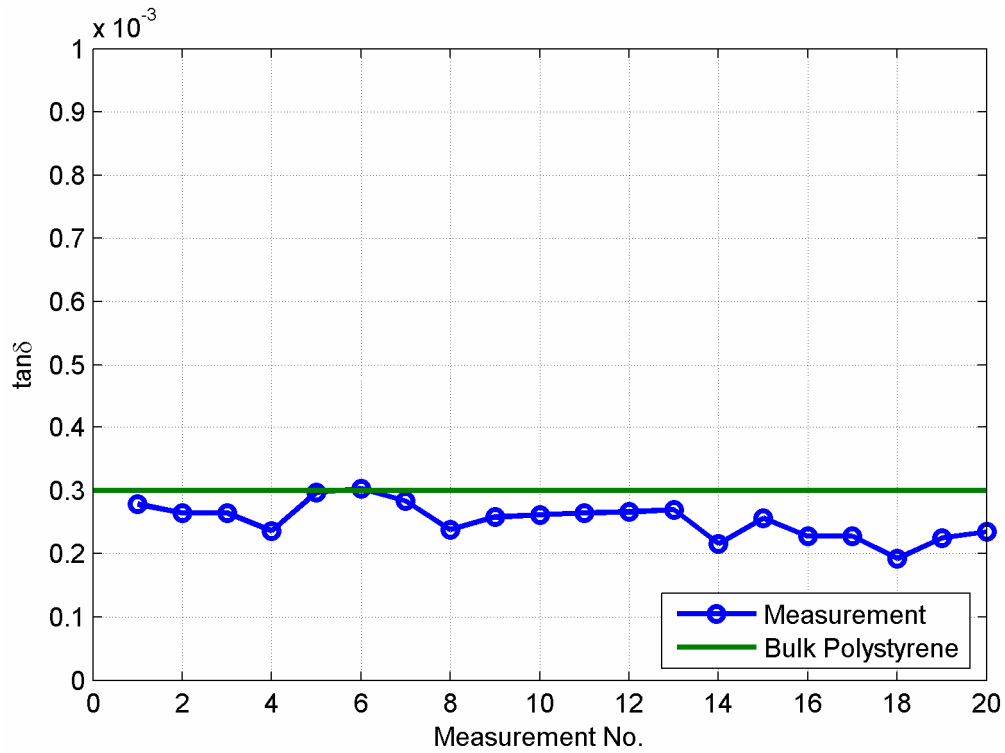
Fig. 19 Measured first resonance loss tangents for 6.22 mm EPS foam.
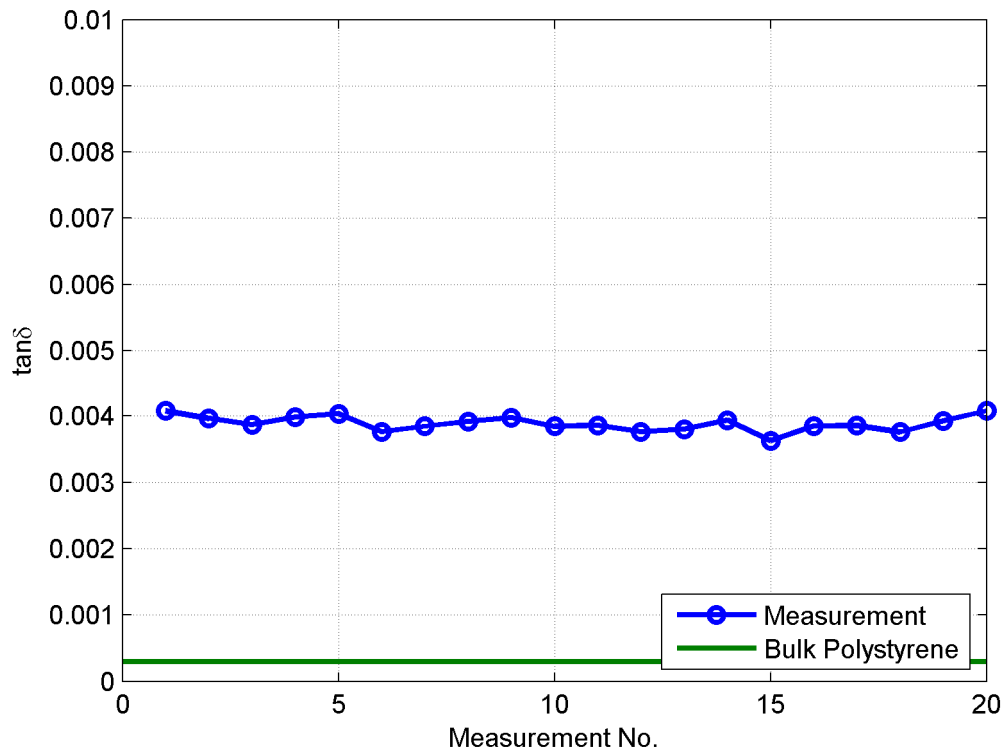
Fig. 20 Measured second resonance loss tangents for 6.22 mm EPS foam.

4.2.3. Uncertainty Analysis

There are two primary sources of error in the measurements presented in the above sections. Measurement errors and resolution effects affect both the planar and suspended ring resonator measurements. In addition, geometric errors occur in the measurement of the air gap between the sample and the suspended ring resonator. Both of these types of errors contribute to the uncertainty in the measurements presented above. This section will focus on the uncertainty in the values of ε_r determined for samples measured using the suspended ring resonator.

The resolution of the S_{21} measurements taken of the device in Fig. 12 contributes to uncertainty in the ε_r measurements made with that device. As previously noted, the measurements were taken over a 40 MHz band with 1601 points and results in a frequency resolution of:

$$f_{\text{step}} = \frac{40\,\text{MHz}}{1601-1} = 25\,\text{kHz} \tag{77}$$

The maximum single-sided error introduced by f_{step} is then

$$
\begin{aligned}
\delta_{\text{step},\varepsilon_r} &= a_3\left(f_\Delta + f_{\text{step}}\right)^3 + a_2\left(f_\Delta + f_{\text{step}}\right)^2 + a_1\left(f_\Delta + f_{\text{step}}\right) + a_0 \\
&\quad - a_3 f_\Delta^3 - a_2 f_\Delta^2 - a_1 f_\Delta - a_0 \\
&= 3a_3\left(f_\Delta^2 f_{\text{step}} + f_\Delta f_{\text{step}}^2\right) + a_3 f_{\text{step}}^3 + 2a_2 f_\Delta f_{\text{step}} + a_2 f_{\text{step}}^2 + a_1 f_{\text{step}}
\end{aligned}
\tag{78}
$$

For the measurements shown in Fig. 15 and Fig. 16, the first resonance exhibited a mean shift of 4.541 MHz, resulting in a maximum single-sided error due to f_{step} of 25 kHz of 1.374×10^{-4} in ε_r. At the second resonance, which exhibited an average shift of 7.291 MHz, the maximum single-sided error due to f_{step} is 6.816×10^{-5}.

Estimating the effect of finite measurement resolution on Q factor measurements is more difficult, due to the fact that Q factor is a derived measurement equal to the ratio of resonance frequency to 3 dB bandwidth. The maximum step in a Q factor measurement due to f_{step} is

$$Q_{step} = \frac{f_{res} + f_{step}}{BW_{3dB} - 2f_{step}} - Q = \frac{QBW_{3dB} + f_{step}}{BW_{3dB} - 2f_{step}} - Q \tag{79}$$

where Q is the measured Q factor and BW_{3dB} is the measured 3dB bandwidth. For the measurements shown in Fig. 19, the mean Q is 149.90 and mean BW_{3dB} is 10.03 MHz. The maximum error in $\tan\delta$ due to f_{step} is then

$$\begin{aligned}
\delta_{step,\tan\delta} &= a_3\left(Q_\Delta + Q_{step}\right)^3 + a_2\left(Q_\Delta + Q_{step}\right)^2 + a_1\left(Q_\Delta + Q_{step}\right) + a_0 \\
&\quad - a_3 Q_\Delta^3 - a_2 Q_\Delta^2 - a_1 Q_\Delta - a_0 \\
&= 3a_3\left(Q_\Delta^2 Q_{step} + Q_\Delta Q_{step}^2\right) + a_3 Q_{step}^3 + 2a_2 Q_\Delta Q_{step} + a_2 Q_{step}^2 + a_1 Q_{step}
\end{aligned} \tag{80}$$

where Q_Δ is the measured shift in Q factor.

For the measurements shown in Fig. 19, the mean shift in Q factor was 0.3530 and f_{step} was 12.5 kHz, resulting in a maximum error in $\tan\delta$ due to f_{step} of 6.325 x 10^{-5}.

Uncertainty in the measurement of the air gap will affect the values of the coefficients a_i. Assuming that the air gap thickness g_{meas} is bounded by $[g_{low}, g_{high}]$ and that the coefficients associated with an air gap of g_x are $a_{i,x}$, the following bounds on the error due to air gap uncertainty can be assumed:

$$\begin{aligned}
\delta_{f,high} &= a_{3,high} f_\Delta^3 + a_{2,high} f_\Delta^2 + a_{1,high} f_\Delta + a_{0,high} \\
&\quad - a_{3,meas} f_\Delta^3 - a_{2,meas} f_\Delta^2 - a_{1,meas} f_\Delta - a_{0,meas}
\end{aligned} \tag{81}$$

$$\begin{aligned}
\delta_{f,low} &= a_{3,meas} f_\Delta^3 + a_{2,meas} f_\Delta^2 + a_{1,meas} f_\Delta + a_{0,meas} \\
&\quad - a_{3,low} f_\Delta^3 - a_{2,low} f_\Delta^2 - a_{1,low} f_\Delta - a_{0,low}
\end{aligned} \tag{82}$$

For the first resonance measurements in Fig. 15 with uncertainty in the air gap of ±0.3 mm, $\delta_{f,high}$ is 2.697 x 10^{-3} and $\delta_{f,low}$ is 2.846 x 10^{-3}. For the second resonance measurements in Fig. 16 with ±0.3 mm uncertainty in the air gap measurement, $\delta_{f,high}$ is 2.140 x 10^{-3} and $\delta_{f,low}$ is 2.262 x 10^{-3}.

Uncertainty in the measurement of the air gap affects measurement of the loss tangent in the same way that it affects measurement of the dielectric constant. Assuming that the air gap thickness g_{meas} is bounded by [g_{low}, g_{high}] and that the coefficients associated with an air gap of g_x are $a_{i,x}$, the following bounds on the error due to air gap uncertainty can be assumed:

$$\delta_{\tan\delta,high} = a_{3,high}Q_\Delta^3 + a_{2,high}Q_\Delta^2 + a_{1,high}Q_\Delta + a_{0,high}$$
$$- a_{3,meas}Q_\Delta^3 - a_{2,meas}Q_\Delta^2 - a_{1,meas}Q_\Delta - a_{0,meas}$$

(83)

$$\delta_{\tan\delta,low} = a_{3,meas}Q_\Delta^3 + a_{2,meas}Q_\Delta^2 + a_{1,meas}Q_\Delta + a_{0,meas}$$
$$- a_{3,low}Q_\Delta^3 - a_{2,low}Q_\Delta^2 - a_{1,low}Q_\Delta - a_{0,low}$$

(84)

For the first resonance measurements in Fig. 19 with air gap uncertainty of ±0.3 mm, $\delta_{\tan\delta,high}$ is 9.276×10^{-6} and $\delta_{\tan\delta,low}$ is 1.011×10^{-5}.

Measurement uncertainty in the frequency of resonances and the size of the air gap between the sample and ring contribute to potential error in the measured dielectric constants and loss tangents. For the dielectric constant measurements, air gap size uncertainty dominates and introduces maximum errors into ε_r measurements on the order of 10^{-3}. For loss tangent measurements, frequency step error dominates and introduces maximum errors on the order of 10^{-5}.

5. Conclusion

The dielectric constant and loss tangent of materials are important inputs to RF engineering tasks. Many methods for the measurement of these properties are available, and these methods are based on a diverse set of tools including direct scattering parameter measurements, transmission line and waveguide methods, and resonant structure analysis.

I have developed a method for determining the dielectric constant and loss tangent of arbitrary low dielectric constant materials based on a suspended ring resonator device. The suspension of the ring above the sample material under test maintains strong interactions between the fields of the ring resonator and the sample material and produces accurate results. Using basic network circuit analysis techniques I have analyzed the behavior of the suspended ring resonator with respect to the S_{21} parameter. The S_{21} model includes the effects of feed gaps and radiation from the ring. The magnitude of the calculated S_{21} parameter is compared to measurements of a real device to determine the dielectric constant and loss tangent of EPS foam. The measured values of dielectric constant match closely with other sources from the literature.

References

[1] M. A. Plonus, "Theoretical investigations of scattering from plastic foams," *IEEE Trans. Antennas and Propagation*, vol. 13, no. 1, pp. 88-94, Jan. 1965.

[2] E. F. Knott, "Dielectric constant of plastic foams," *IEEE Trans. Antennas and Propagation*, vol. 41, no. 8, pp. 1167-1171, Aug. 1993.

[3] J. A. Berrie and G. L. Wilson, "Design of target support columns using EPS foams," *IEEE Antennas and Propagation Magazine*, vol. 45, no. 1, pp. 198-206, Feb. 2003.

[4] G. Zhao, M. ter Mors, W. T. Wenckebach, and P. C. M. Planken, "THz near-invisible materials: the dielectric properties of polystyrene foam," *Lasers and Electro-Optics, 2002. CLEO '02*, vol. 1, p. 237, 2002.

[5] G. Zhao, M. ter Mors, W. T. Wenckebach, and P.C.M. Planken, "Terahertz dielectric properties of polystyrene foam," *J. Opt. Soc. Am. B*, vol. 19, no. 6, pp. 1476-1479, June 2002.

[6] B. Riddle, J. Baker-Jarvis, and J. Krupka, "Complex permittivity measurements of common plastics over variable temperatures," *IEEE Trans. Microwave Theory and Techniques*, vol. 51, no. 3, pp. 727-733, Mar. 2003.

[7] J. Friedman, "Dielectric-Constant Measuring Apparatus," U.S. Patent 3,965,416, June 22, 1976.

[8] B. R. De and M. A. Nelson, "Method and Apparatus for Broadband Measurement of Dielectric Properties," U.S. Patent 5,132,623, July 21, 1992.

[9] M. M. Neel and F. J. Schiavone, "Dielectric Constant Probe Assembly and Apparatus and Method," U.S. Patent 5,157,337, October 20, 1992.

[10] S. Nagata, S. Miyamoto, and F. Okada, "Method and Device for Measuring Dielectric Constant," U.S. Patent 6,496,018, Dec. 17, 2002.

[11] N. Gagnon, J. Shaker, L. Roy, A. Petosa, and P. Berini. "Low-cost free-space measurement of dielectric constant at Ka band." *IEEE Proc. Microwaves, Antennas, and Propagation*, vol. 151, no. 3, pp. 271-276, 21 Jun. 2004.

[12] D. K. Ghodgaonkar, V. V. Varadan, and V. K. Varadan. "A free-space method for measurement of dielectric constants and loss tangents at microwave frequencies." *IEEE Trans. Instrumentation and Measurement*, vol. 38, no. 3, pp. 789-793, Jun. 1989.

[13] A. Muqaibel and A. Safaai-Jazi. "New formulation for evaluating complex permittivity of low-loss materials." *Proc. IEEE Antennas and Propagation Soc. Int'l Symp.*, vol. 4, 22-27 June 2003, pp. 631-634.

[14] M. D. Deshpande, C. J. Reddy, P. I. Tiemsin, and R. Cravey. "A new approach to estimate complex permittivity of dielectric materials at microwave frequeincies using waveguide measurements." *IEEE Trans. Microwave Theory and Techniques*, vol. 45, no. 3, pp. 359-366, March 1997.

[15] Z. Abbas, R. D. Pollard, R. W. Kelsall. "Further extensions to rectangular dielectric waveguide technique for dielectric measurements." *Proc. IEEE Instrumentation and Measurement Conf.*, vol. 1, 19-21 May 1997, Ottawa, Canada, pp. 44-46.

[16] Y.-S. Yeh, J.-T. Lue, and Z.-R. Zheng. "Measurement of the dielectric constants of metallic nanoparticles embedded in a paraffin rod at microwave frequencies." *IEEE Trans. Microwave Theory and Techniques*, vol. 53, no. 5, pp. 1756-1760, May 2005.

[17] K. Sarabandi and F. T. Ulaby. "Technique for measuring the dielectric constant of thin materials." *IEEE Trans. Instrumentation and Measurement*, vol. 37, no. 4, pp. 631-636, Dec. 1988.

[18] A. Baysar and J. L. Kuester, "Dielectric property measurements of materials using the cavity technique," *IEEE Trans. Microwave Theory and Techniques*, vol. 40, no. 11, pp. 2108-2110, Nov. 1992.

[19] R. Keam and A. D. Green, "Measurement of complex dielectric permittivity at microwave frequencies using a cylindrical cavity," *IEE Electronics Letters*, vol. 31, no. 3, pp. 212-214, Feb. 2, 1995.

[20] S. O. Nelson, "Measurement and calculation of powdered mixture permittivities," *IEEE Trans. Instrumentation and Measurement*, vol. 50, no. 5, pp. 1066-1070, Oct. 2001.

[21] P. A. Bernard and J. M. Gautray, "Measurement of dielectric constant using a microstrip ring resonator," *IEEE Trans. Microwave Theory and Techniques*, vol. 39, no. 3, pp. 592-595, March 1991.

[22] E. Semouchkina, W. Cao, and M. Lanagan, "High frequency permittivity determination by spectra simulation and measurement of microstrip ring resonators," *IEE Electronics Letters*, vol. 36, no. 11, pp. 956-958, May 25, 2000.

[23] J.-M. Heinola, P. Silventoinen, K. Lätti, M. Kettunen, J.-P. Ström, "Determination of dielectric constant and dissipation factor of a printed circuit board material using a microstrip ring resonator structure," *Proc. 15th Int'l Conf. Microwave, Radar and Wireless Comm.*, vol. 1, May 17-19, 2004, pp. 202-205.

[24] M. Saed, "Measurement of the complex permittivity of low-loss microwave substrates using aperture-coupled microstrip resonators," *IEEE Trans. Microwave Theory and Techniques*, vol. 41, no. 8, pp. 1343-1348, August 1993.

[25] Y. Kantor, "Dielectric constant measurements using printed circuit techniques at microwave frequencies," *Proc. 9th Mediterranean Electrotechnical Conf.*, vol. 1, May 18-20, 1998, pp. 101-105.

[26] Sz. Maj and M. W. Modelski, "Application of a dielectric resonator on microstrip line for measurement of complex permittivity," *1984 IEEE MTT-S Int'l Microwave Symp. Dig.*, vol. 84, no. 1, May 1984, pp. 525-527.

[27] A. E. Fathy, V. A. Pendrick, B. D. Geller, S. M. Perlow, E. S. Tormey, A. Prabhu, and S. Tani, "An innovative semianalytical technique for ceramic evaluation at microwave frequencies," *IEEE Trans. Microwave Theory and Techniques*, vol. 50, no. 10, pp. 2247-2252, Oct. 2002.

[28] C.-C. Yu and K. Chang, "Transmission-line analysis of a capacitively coupled microstrip-ring resonator," *IEEE Trans. Microwave Theory and Techniques*, vol. 45, no. 11, pp. 2018-2024, Nov. 1997.

[29] L.-H. Hsieh and K. Chang, "Equivalent lumped elements G, L, C, and unload Q's of closed- and open-loop ring resonators," *IEEE Trans. Microwave Theory and Techniques*, vol. 50, no. 2, pp. 453-460, Feb. 2002.

[30] B. S. Virdee and C. Grassopoulos, "Folded microstrip resonator," *2003 IEEE MTT-S Int'l Microwave Symp. Dig.*, vol. 3, June 8-13, 2003, pp. 2161-2164.

[31] R. Singh, A. De, and R. S. Yadava, "A simple method for measuring dielectric constant at microwave frequency," *1990 Conf. Precision Electromagnetic Measurements Dig.*, 11-14 Jun. 1990, pp. 236-237.

[32] H. G. Akhavan and D. Mirshekar-Syahkal, "Slot antennas for measurement of properties of dielectrics at microwave frequencies," *Proc. IEE Nat'l Conf. Antennas and Propagation*, 30 Mar.-1 Apr. 1999, pp. 8-11.

[33] M. Bogosoanovich, "Microstrip patch sensor for measurement of the permittivity of homogenous dielectric materials," *IEEE Trans. Instrumentation and Measurement*, vol. 49, no. 5, pp. 1144-1148, Oct. 2000.

[34] A. N. Deleniv and S. Gevorgian, "Open resonator technique for measuring multilayered dielectric plates," *IEEE Trans. Microwave Theory and Techniques*, vol. 53, no. 9, pp. 2908-2916, Sep. 2005.

[35] R. Inoue, Y. Odate, E. Tanabe, H. Kitano, and A. Maeda, "Data analysis of the extraction of dielectric proerties from insulating substrates utilizing the evanaesnt perturbation method," *IEEE Trans. Microwave Theory and Techniques*, vol. 54, no. 2, pp. 522-532, Feb. 2006.

[36] R. Ludwig and P. Bretchko, "Single- and multiport networks" in <u>RF Circuit Design: Theory and Applications</u>, Upper Saddle River, NJ: Prentice Hall, 2000.

[37] D. M. Pozar, "Microwave network analysis" in <u>Microwave Engineering</u>, 3rd ed., Hoboken, NJ: John Wiley and Sons, Inc., 2005.

[38] R. Garg and I. J. Bahl, "Microstrip discontinuities," *Int'l J. Electronics*, vol. 45, pp. 81-87, 1978.

[39] R. P. Owens, "Curvature effect in microstrip ring resonator," *IEE Electronics Letters*, vol. 12, no. 14, pp. 356-357, Jul. 1976.

[40] R. Ludwig and P. Bretchko, "Transmission line analysis" in <u>RF Circuit Design: Theory and Applications</u>, Upper Saddle River, NJ: Prentice Hall, 2000.

[41] D. M. Pozar, "Transmission lines and waveguides" in <u>Microwave Engineering</u>, 3rd ed., Hoboken, NJ: John Wiley and Sons, Inc., 2005.

[42] J. Svačina, "A simple quasi-static determination of basic parameters of multilayer microstrip and coplanar waveguide," *IEEE Microwave and Guided Wave Letters*, vol. 2, no. 10, pp. 385-387, Oct. 1992.

[43] J. Svačina, "Analysis of multilayer microstrip lines by a conformal mapping method," *IEEE Trans. Microwave Theory and Techniques*, vol. 40, no. 4, pp. 769-772, Apr. 1992.

[44] D. A. Hill, D. G. Camell, K. H. Cavcey, and G. H. Koepke, "Radiated emissions and immunity of microstrip transmission lines: theory and reverberation chamber measurements," *IEEE Trans. Electromagnetic Compatibility*, vol. 38, no. 2, pp. 165-172, May 1996.

[45] D. M. Pozar, "Transmission line theory" in <u>Microwave Engineering</u>, 3rd ed., Hoboken, NJ: John Wiley and Sons, Inc., 2005.

[46] Isola Laminate Systems Corp., "Datasheet 5040/2/02," Isola Laminate Systems Corp., 2002.

Appendix A MATLAB Codes

A.1 RingSandwich.m

```
function [diff, fMax_air, fMax_sample, BW_air, BW_sample] = ...
         RingSandwich(e, d, t, gap, res);
% This function takes in following parameters:
% e   - dielectric constant of sample layer
% d   - loss tangent of sample layer
% t   - thickness of sample layer [m]
% gap - thickness of air gap layer [m]
% res - the number of the desired resonance (1, 2, ...)
%
% This function returns the follow parameters:
% diff        - the difference between fMax_air and fMax_sample
% fMax_air    - the location of the desired resonance without the sample
% fMax_sample - the location of the desired resonance with the sample

% Constants
eps_air        = 1.00059;
mu0            = pi*4e-7;
eps0           = 8.85418782e-12;
n0             = sqrt(mu0/eps0);
w              = 2.2e-3;
s              = 0.25e-3;
r              = 25.9e-3;
len            = pi*r;
f_minstep      = 1e2;
f_fact         = 0.9;
N              = 3;
maxiter        = 100;

%   Dielectric Data/Resonance Frequency for air (no sample)
m       = 2;    % ring is above second layer
T       = [62e-3*2.54e-2 (t + gap) 62e-3*2.54e-2];
E       = [4.25          eps_air   4.25  eps_air];
D       = [0.016         0         0.016 0];
[line_Eeff line_Z0 line_Vp] = microstrip(w, T(1), E(1)*(1 - j*D(1)));
[ring_Eeff ring_Z0 ring_Vp] = microstrip_nlayer(w, m, T, E.*(1 - j*D));
ring_F0 = res*real(ring_Vp/(2*len));
[Cp Cg]    = gap_capacitance(w, T(1), s, E(1));
fMax_air = 0;
found = 0;
f_start = ring_F0*f_fact;
f_stop  = ring_F0;
niter = 0;
while (0 == found)
    niter = niter + 1;
    if (maxiter == niter)
        error('too many iterations!');
    end
    f_step      = ceil((f_stop - f_start)/(N*f_minstep))*f_minstep;
    f_wide      =
floor(f_start/f_step)*f_step:f_step:ceil(f_stop/f_step)*f_step;
    omega       = 2*pi*f_wide;
```

```
    Er = E(1:end - 1)*T(1:end)'/sum(T(1:end));
    EffRad = [];
    for i = 1:length(f_wide)
        EffRad(end + 1) = RingRadiation(Er, real(ring_Eeff), real(ring_Z0),
len, sum(T(1:m)), f_wide(i));
    end
    y            = j*omega.*sqrt(mu0*eps0*ring_Eeff) - EffRad/(2*len);

    S21          = 8*line_Z0*ring_Z0*Cg^2*exp(-y*len).*omega.^2./(-
4+4*j*line_Z0^2*omega.^3*Cp*ring_Z0*Cg^2+4*line_Z0^2*omega.^2*Cp^2-
8*line_Z0^2*omega.^2*Cg.*exp(-
2*y*len)*Cp+8*ring_Z0*omega.^2*Cp*Cg*line_Z0.*exp(-
2*y*len)+8*line_Z0^2*omega.^2*Cp*Cg+ring_Z0^2*omega.^2*Cg^2+8*omega.^2*line_Z
0*ring_Z0*Cg*Cp+4*line_Z0^2*omega.^2*Cg^2+4*omega.^2*line_Z0*ring_Z0*Cg^2.*ex
p(-
2*y*len)+4*j*line_Z0^2*omega.^3*Cp^2*ring_Z0*Cg+line_Z0^2*omega.^4*Cp^2*ring_
Z0^2*Cg^2.*exp(-2*y*len)-line_Z0^2*omega.^4*Cp^2*ring_Z0^2*Cg^2-
4*line_Z0^2*omega.^2*Cg^2.*exp(-2*y*len)-4*line_Z0^2*omega.^2*Cp^2.*exp(-
2*y*len)-ring_Z0^2*omega.^2*Cg^2.*exp(-2*y*len)+4.*exp(-
2*y*len)+4*omega.^2*line_Z0*ring_Z0*Cg^2+2*j*ring_Z0^2*omega.^3*Cp*Cg^2*line_
Z0-4*j*ring_Z0*omega*Cg-8*j*omega*line_Z0*Cg-
8*j*omega*line_Z0*Cp+4*j*line_Z0^2*omega.^3*Cp^2*ring_Z0*Cg.*exp(-
2*y*len)+4*j*line_Z0^2*omega.^3*Cp*ring_Z0*Cg^2.*exp(-
2*y*len)+8*j*omega*line_Z0.*exp(-2*y*len)*Cp+8*j*omega*line_Z0.*exp(-
2*y*len)*Cg-4*j*ring_Z0*omega*Cg.*exp(-2*y*len)-
2*j*ring_Z0^2*omega.^3*Cp*Cg^2*line_Z0.*exp(-2*y*len));
    ind          = find(max(abs(S21)) == abs(S21));
    fMax_air     = mean(f_wide(ind));
    if (fMax_air <= f_start)
        f_stop = f_start + f_step;
        f_start = f_stop - N*f_step;
    elseif (fMax_air >= f_stop)
        f_start = f_stop - f_step;
        f_stop = f_start + N*f_step;
    elseif (f_step > f_minstep)
        f_start = f_wide(ind(1)) - f_step/2;
        f_stop = f_wide(ind(end)) + f_step/2;
    else
        found = 1;
    end
end

if (fMax_air <= f_start || fMax_air >= f_stop)
    error('fMax_air not in (f_start, f_stop)!');
end

if (3 < nargout)
    target = 20*log10(max(abs(S21))*sqrt(2)/2);
    f3dBL_air = 0;
    found = 0;
    f_start = fMax_air - 10e6;
    f_stop  = fMax_air;
    niter = 0;
    while (0 == found)
        niter = niter + 1;
        if (maxiter == niter)
            error('too many iterations!');
```

```
        end
        f_step      = ceil((f_stop - f_start)/(N*f_minstep))*f_minstep;
        f_wide      =
floor(f_start/f_step)*f_step:f_step:ceil(f_stop/f_step)*f_step;
        omega       = 2*pi*f_wide;

        Er = E(1:end - 1)*T(1:end)'/sum(T(1:end));
        EffRad = [];
        for i = 1:length(f_wide)
            EffRad(end + 1) = RingRadiation(Er, real(ring_Eeff),
real(ring_Z0), len, sum(T(1:m)), f_wide(i));
        end
        y           = j*omega.*sqrt(mu0*eps0*ring_Eeff) - EffRad/(2*len);

        S21         = 8*line_Z0*ring_Z0*Cg^2*exp(-y*len).*omega.^2./(-
4+4*j*line_Z0^2*omega.^3*Cp*ring_Z0*Cg^2+4*line_Z0^2*omega.^2*Cp^2-
8*line_Z0^2*omega.^2*Cg.*exp(-
2*y*len)*Cp+8*ring_Z0*omega.^2*Cp*Cg*line_Z0.*exp(-
2*y*len)+8*line_Z0^2*omega.^2*Cp*Cg+ring_Z0^2*omega.^2*Cg^2+8*omega.^2*line_Z
0*ring_Z0*Cg*Cp+4*line_Z0^2*omega.^2*Cg^2+4*omega.^2*line_Z0*ring_Z0*Cg^2.*ex
p(-
2*y*len)+4*j*line_Z0^2*omega.^3*Cp^2*ring_Z0*Cg+line_Z0^2*omega.^4*Cp^2*ring_
Z0^2*Cg^2.*exp(-2*y*len)-line_Z0^2*omega.^4*Cp^2*ring_Z0^2*Cg^2-
4*line_Z0^2*omega.^2*Cg^2.*exp(-2*y*len)-4*line_Z0^2*omega.^2*Cp^2.*exp(-
2*y*len)-ring_Z0^2*omega.^2*Cg^2.*exp(-2*y*len)+4.*exp(-
2*y*len)+4*omega.^2*line_Z0*ring_Z0*Cg^2+2*j*ring_Z0^2*omega.^3*Cp*Cg^2*line_
Z0-4*j*ring_Z0*omega*Cg-8*j*omega*line_Z0*Cg-
8*j*omega*line_Z0*Cp+4*j*line_Z0^2*omega.^3*Cp^2*ring_Z0*Cg.*exp(-
2*y*len)+4*j*line_Z0^2*omega.^3*Cp*ring_Z0*Cg^2.*exp(-
2*y*len)+8*j*omega*line_Z0.*exp(-2*y*len)*Cp+8*j*omega*line_Z0.*exp(-
2*y*len)*Cg-4*j*ring_Z0*omega*Cg.*exp(-2*y*len)-
2*j*ring_Z0^2*omega.^3*Cp*Cg^2*line_Z0.*exp(-2*y*len));
        ind         = find(min(abs(20*log10(abs(S21)) - target)) ==
abs(20*log10(abs(S21)) - target));
        f3dBL_air   = mean(f_wide(ind));
        if (f3dBL_air <= f_start)
            f_stop = f_start + f_step;
            f_start = f_stop - N*f_step;
        elseif (f3dBL_air >= f_stop & (f_start + N*f_step) <= fMax_air)
            f_start = f_stop - f_step;
            f_stop = f_start + N*f_step;
        elseif (f_step > f_minstep)
            f_stop = min(fMax_air, f_wide(ind(end)) + f_step/2);
            f_start = f_stop - range(f_wide(ind)) - f_step;
        else
            found = 1;
        end
    end

    if (f3dBL_air <= f_start || f3dBL_air >= f_stop)
        error('f3dBL_air not in (f_start, f_stop)!');
    end

    f3dBU_air = 0;
    found = 0;
    f_start = fMax_air;
    f_stop  = fMax_air + 10e6;
```

```
    niter = 0;
    while (0 == found)
        niter = niter + 1;
        if (maxiter == niter)
            error('too many iterations!');
        end
        f_step      = ceil((f_stop - f_start)/(N*f_minstep))*f_minstep;
        f_wide      =
floor(f_start/f_step)*f_step:f_step:ceil(f_stop/f_step)*f_step;
        omega       = 2*pi*f_wide;

        Er = E(1:end - 1)*T(1:end)'/sum(T(1:end));
        EffRad = [];
        for i = 1:length(f_wide)
            EffRad(end + 1) = RingRadiation(Er, real(ring_Eeff),
real(ring_Z0), len, sum(T(1:m)), f_wide(i));
        end
        y           = j*omega.*sqrt(mu0*eps0*ring_Eeff) - EffRad/(2*len);

        S21         = 8*line_Z0*ring_Z0*Cg^2*exp(-y*len).*omega.^2./(-
4+4*j*line_Z0^2*omega.^3*Cp*ring_Z0*Cg^2+4*line_Z0^2*omega.^2*Cp^2-
8*line_Z0^2*omega.^2*Cg.*exp(-
2*y*len)*Cp+8*ring_Z0*omega.^2*Cp*Cg*line_Z0.*exp(-
2*y*len)+8*line_Z0^2*omega.^2*Cp*Cg+ring_Z0^2*omega.^2*Cg^2+8*omega.^2*line_Z
0*ring_Z0*Cg*Cp+4*line_Z0^2*omega.^2*Cg^2+4*omega.^2*line_Z0*ring_Z0*Cg^2.*ex
p(-
2*y*len)+4*j*line_Z0^2*omega.^3*Cp^2*ring_Z0*Cg+line_Z0^2*omega.^4*Cp^2*ring_
Z0^2*Cg^2.*exp(-2*y*len)-line_Z0^2*omega.^4*Cp^2*ring_Z0^2*Cg^2-
4*line_Z0^2*omega.^2*Cg^2.*exp(-2*y*len)-4*line_Z0^2*omega.^2*Cp^2.*exp(-
2*y*len)-ring_Z0^2*omega.^2*Cg^2.*exp(-2*y*len)+4.*exp(-
2*y*len)+4*omega.^2*line_Z0*ring_Z0*Cg^2+2*j*ring_Z0^2*omega.^3*Cp*Cg^2*line_
Z0-4*j*ring_Z0*omega*Cg-8*j*omega*line_Z0*Cg-
8*j*omega*line_Z0*Cp+4*j*line_Z0^2*omega.^3*Cp^2*ring_Z0*Cg.*exp(-
2*y*len)+4*j*line_Z0^2*omega.^3*Cp*ring_Z0*Cg^2.*exp(-
2*y*len)+8*j*omega*line_Z0.*exp(-2*y*len)*Cp+8*j*omega*line_Z0.*exp(-
2*y*len)*Cg-4*j*ring_Z0*omega*Cg.*exp(-2*y*len)-
2*j*ring_Z0^2*omega.^3*Cp*Cg^2*line_Z0.*exp(-2*y*len));
        ind         = find(min(abs(20*log10(abs(S21)) - target)) ==
abs(20*log10(abs(S21)) - target));
        f3dBU_air   = mean(f_wide(ind));
        if (f3dBU_air <= f_start & (f_stop - N*f_step) >= fMax_air)
            f_stop = f_start + f_step;
            f_start = f_stop - N*f_step;
        elseif (f3dBU_air >= f_stop)
            f_start = f_stop - f_step;
            f_stop = f_start + N*f_step;
        elseif (f_step > f_minstep)
            f_start = max(fMax_air, f_wide(ind(1)) - f_step/2);
            f_stop = f_start + range(f_wide(ind)) + f_step;
        else
            found = 1;
        end
    end

    if (f3dBU_air <= f_start || f3dBU_air >= f_stop)
        error('f3dBU_air not in (f_start, f_stop)!');
    end
```

```
    BW_air = (f3dBU_air - f3dBL_air)/1e9;
end


%    Dielectric Data/Resonance Frequency for sample
m       = 3;     % ring is above third layer
T       = [62e-3*2.54e-2    t       gap     62e-3*2.54e-2];
E       = [4.25             e       eps_air  4.25  eps_air];
D       = [0.016            d       0        0.016 0];
[line_Eeff line_Z0 line_Vp] = microstrip(w, T(1), E(1)*(1 - j*D(1)));
[ring_Eeff ring_Z0 ring_Vp] = microstrip_nlayer(w, m, T, E.*(1 - j*D));
ring_F0 = res*real(ring_Vp/(2*len));
[Cp Cg]      = gap_capacitance(w, T(1), s, E(1));
fMax_sample = 0;
found = 0;
f_start = ring_F0*f_fact;
f_stop  = ring_F0;
niter = 0;
while (0 == found)
    niter = niter + 1;
    if (maxiter == niter)
        error('too many iterations!');
    end
    f_step      = ceil((f_stop - f_start)/(N*f_minstep))*f_minstep;
    f_wide      =
floor(f_start/f_step)*f_step:f_step:ceil(f_stop/f_step)*f_step;
    omega       = 2*pi*f_wide;

    Er = E(1:end - 1)*T(1:end)'/sum(T(1:end));
    EffRad = [];
    for i = 1:length(f_wide)
        EffRad(end + 1) = RingRadiation(Er, real(ring_Eeff), real(ring_Z0),
len, sum(T(1:m)), f_wide(i));
    end
    y           = j*omega.*sqrt(mu0*eps0*ring_Eeff) - EffRad/(2*len);

    S21         = 8*line_Z0*ring_Z0*Cg^2*exp(-y*len).*omega.^2./(-
4+4*j*line_Z0^2*omega.^3*Cp*ring_Z0*Cg^2+4*line_Z0^2*omega.^2*Cp^2-
8*line_Z0^2*omega.^2*Cg.*exp(-
2*y*len)*Cp+8*ring_Z0*omega.^2*Cp*Cg*line_Z0.*exp(-
2*y*len)+8*line_Z0^2*omega.^2*Cp*Cg+ring_Z0^2*omega.^2*Cg^2+8*omega.^2*line_Z
0*ring_Z0*Cg*Cp+4*line_Z0^2*omega.^2*Cg^2+4*omega.^2*line_Z0*ring_Z0*Cg^2.*ex
p(-
2*y*len)+4*j*line_Z0^2*omega.^3*Cp^2*ring_Z0*Cg+line_Z0^2*omega.^4*Cp^2*ring_
Z0^2*Cg^2.*exp(-2*y*len)-line_Z0^2*omega.^4*Cp^2*ring_Z0^2*Cg^2-
4*line_Z0^2*omega.^2*Cg^2.*exp(-2*y*len)-4*line_Z0^2*omega.^2*Cp^2.*exp(-
2*y*len)-ring_Z0^2*omega.^2*Cg^2.*exp(-2*y*len)+4.*exp(-
2*y*len)+4*omega.^2*line_Z0*ring_Z0*Cg^2+2*j*ring_Z0^2*omega.^3*Cp*Cg^2*line_
Z0-4*j*ring_Z0*omega*Cg-8*j*omega*line_Z0*Cg-
8*j*omega*line_Z0*Cp+4*j*line_Z0^2*omega.^3*Cp^2*ring_Z0*Cg.*exp(-
2*y*len)+4*j*line_Z0^2*omega.^3*Cp*ring_Z0*Cg^2.*exp(-
2*y*len)+8*j*omega*line_Z0.*exp(-2*y*len)*Cp+8*j*omega*line_Z0.*exp(-
2*y*len)*Cg-4*j*ring_Z0*omega*Cg.*exp(-2*y*len)-
2*j*ring_Z0^2*omega.^3*Cp*Cg^2*line_Z0.*exp(-2*y*len));
    ind         = find(max(abs(S21)) == abs(S21));
    fMax_sample = mean(f_wide(ind));
    if (fMax_sample <= f_start)
```

```matlab
        f_stop = f_start + f_step;
        f_start = f_stop - N*f_step;
    elseif (fMax_sample >= f_stop)
        f_start = f_stop - f_step;
        f_stop = f_start + N*f_step;
    elseif (f_step > f_minstep)
        f_start = f_wide(ind(1)) - f_step/2;
        f_stop = f_wide(ind(end)) + f_step/2;
    else
        found = 1;
    end
end

if (fMax_sample <= f_start || fMax_sample >= f_stop)
    error('fMax_sample not in (f_start, f_stop)!');
end

if (3 < nargout)
    target = 20*log10(max(abs(S21))*sqrt(2)/2);
    f3dBL_sample = 0;
    found = 0;
    f_start = fMax_sample - 10e6;
    f_stop  = fMax_sample;
    niter = 0;
    while (0 == found)
        niter = niter + 1;
        if (maxiter == niter)
            error('too many iterations!');
        end
        f_step       = ceil((f_stop - f_start)/(N*f_minstep))*f_minstep;
        f_wide       =
floor(f_start/f_step)*f_step:f_step:ceil(f_stop/f_step)*f_step;
        omega        = 2*pi*f_wide;

        Er = E(1:end - 1)*T(1:end)'/sum(T(1:end));
        EffRad = [];
        for i = 1:length(f_wide)
            EffRad(end + 1) = RingRadiation(Er, real(ring_Eeff),
real(ring_Z0), len, sum(T(1:m)), f_wide(i));
        end
        y            = j*omega.*sqrt(mu0*eps0*ring_Eeff) - EffRad/(2*len);

        S21          = 8*line_Z0*ring_Z0*Cg^2*exp(-y*len).*omega.^2./(-
4+4*j*line_Z0^2*omega.^3*Cp*ring_Z0*Cg^2+4*line_Z0^2*omega.^2*Cp^2-
8*line_Z0^2*omega.^2*Cg.*exp(-
2*y*len)*Cp+8*ring_Z0*omega.^2*Cp*Cg*line_Z0.*exp(-
2*y*len)+8*line_Z0^2*omega.^2*Cp*Cg+ring_Z0^2*omega.^2*Cg^2+8*omega.^2*line_Z
0*ring_Z0*Cg*Cp+4*line_Z0^2*omega.^2*Cg^2+4*omega.^2*line_Z0*ring_Z0*Cg^2.*ex
p(-
2*y*len)+4*j*line_Z0^2*omega.^3*Cp^2*ring_Z0*Cg+line_Z0^2*omega.^4*Cp^2*ring_
Z0^2*Cg^2.*exp(-2*y*len)-line_Z0^2*omega.^4*Cp^2*ring_Z0^2*Cg^2-
4*line_Z0^2*omega.^2*Cg^2.*exp(-2*y*len)-4*line_Z0^2*omega.^2*Cp^2.*exp(-
2*y*len)-ring_Z0^2*omega.^2*Cg^2.*exp(-2*y*len)+4.*exp(-
2*y*len)+4*omega.^2*line_Z0*ring_Z0*Cg^2+2*j*ring_Z0^2*omega.^3*Cp*Cg^2*line_
Z0-4*j*ring_Z0*omega*Cg-8*j*omega*line_Z0*Cg-
8*j*omega*line_Z0*Cp+4*j*line_Z0^2*omega.^3*Cp^2*ring_Z0*Cg.*exp(-
2*y*len)+4*j*line_Z0^2*omega.^3*Cp*ring_Z0*Cg^2.*exp(-
```

```
2*y*len)+8*j*omega*line_Z0.*exp(-2*y*len)*Cp+8*j*omega*line_Z0.*exp(-
2*y*len)*Cg-4*j*ring_Z0*omega*Cg.*exp(-2*y*len)-
2*j*ring_Z0^2*omega.^3*Cp*Cg^2*line_Z0.*exp(-2*y*len));
        ind           = find(min(abs(20*log10(abs(S21)) - target)) ==
abs(20*log10(abs(S21)) - target));
        f3dBL_sample    = mean(f_wide(ind));
        if (f3dBL_sample <= f_start)
            f_stop = f_start + f_step;
            f_start = f_stop - N*f_step;
        elseif (f3dBL_sample >= f_stop & (f_start + N*f_step) <= fMax_sample)
            f_start = f_stop - f_step;
            f_stop = f_start + N*f_step;
        elseif (f_step > f_minstep)
            f_stop = min(fMax_sample, f_wide(ind(end)) + f_step/2);
            f_start = f_stop - range(f_wide(ind)) - f_step;
        else
            found = 1;
        end
    end

    if (f3dBL_sample <= f_start || f3dBL_sample >= f_stop)
        error('f3dBL_sample not in (f_start, f_stop)!');
    end

    f3dBU_sample = 0;
    found = 0;
    f_start = fMax_sample;
    f_stop  = f_start + 10e6;
    niter = 0;
    while (0 == found)
        niter = niter + 1;
        if (maxiter == niter)
            error('too many iterations!');
        end
        f_step      = ceil((f_stop - f_start)/(N*f_minstep))*f_minstep;
        f_wide      =
floor(f_start/f_step)*f_step:f_step:ceil(f_stop/f_step)*f_step;
        omega        = 2*pi*f_wide;

        Er = E(1:end - 1)*T(1:end)'/sum(T(1:end));
        EffRad = [];
        for i = 1:length(f_wide)
            EffRad(end + 1) = RingRadiation(Er, real(ring_Eeff),
real(ring_Z0), len, sum(T(1:m)), f_wide(i));
        end
        y            = j*omega.*sqrt(mu0*eps0*ring_Eeff) - EffRad/(2*len);

        S21         = 8*line_Z0*ring_Z0*Cg^2*exp(-y*len).*omega.^2./(-
4+4*j*line_Z0^2*omega.^3*Cp*ring_Z0*Cg^2+4*line_Z0^2*omega.^2*Cp^2-
8*line_Z0^2*omega.^2*Cg.*exp(-
2*y*len)*Cp+8*ring_Z0*omega.^2*Cp*Cg*line_Z0.*exp(-
2*y*len)+8*line_Z0^2*omega.^2*Cp*Cg+ring_Z0^2*omega.^2*Cg^2+8*omega.^2*line_Z
0*ring_Z0*Cg*Cp+4*line_Z0^2*omega.^2*Cg^2+4*omega.^2*line_Z0*ring_Z0*Cg^2.*ex
p(-
2*y*len)+4*j*line_Z0^2*omega.^3*Cp^2*ring_Z0*Cg+line_Z0^2*omega.^4*Cp^2*ring_
Z0^2*Cg^2.*exp(-2*y*len)-line_Z0^2*omega.^4*Cp^2*ring_Z0^2*Cg^2-
4*line_Z0^2*omega.^2*Cg^2.*exp(-2*y*len)-4*line_Z0^2*omega.^2*Cp^2.*exp(-
```

```
2*y*len)-ring_Z0^2*omega.^2*Cg^2.*exp(-2*y*len)+4.*exp(-
2*y*len)+4*omega.^2*line_Z0*ring_Z0*Cg^2+2*j*ring_Z0^2*omega.^3*Cp*Cg^2*line_
Z0-4*j*ring_Z0*omega*Cg-8*j*omega*line_Z0*Cg-
8*j*omega*line_Z0*Cp+4*j*line_Z0^2*omega.^3*Cp^2*ring_Z0*Cg.*exp(-
2*y*len)+4*j*line_Z0^2*omega.^3*Cp*ring_Z0*Cg^2.*exp(-
2*y*len)+8*j*omega*line_Z0.*exp(-2*y*len)*Cp+8*j*omega*line_Z0.*exp(-
2*y*len)*Cg-4*j*ring_Z0*omega*Cg.*exp(-2*y*len)-
2*j*ring_Z0^2*omega.^3*Cp*Cg^2*line_Z0.*exp(-2*y*len));
        ind           = find(min(abs(20*log10(abs(S21)) - target)) ==
abs(20*log10(abs(S21)) - target));
        f3dBU_sample    = mean(f_wide(ind));
        if (f3dBU_sample <= f_start & (f_stop - N*f_step) >= fMax_sample)
            f_stop = f_start + f_step;
            f_start = f_stop - N*f_step;
        elseif (f3dBU_sample >= f_stop)
            f_start = f_stop - f_step;
            f_stop = f_start + N*f_step;
        elseif (f_step > f_minstep)
            f_start = max(fMax_sample, f_wide(ind(1)) - f_step/2);
            f_stop = f_start + range(f_wide(ind)) + f_step;
        else
            found = 1;
        end
    end

    if (f3dBU_sample <= f_start || f3dBU_sample >= f_stop)
        error('f3dBU_sample not in (f_start, f_stop)!');
    end

    BW_sample = (f3dBU_sample - f3dBL_sample)/1e9;
end

fMax_air = fMax_air/1e9;
fMax_sample = fMax_sample/1e9;
diff = fMax_air - fMax_sample;
```

A.2 microstrip.m

```
function [Eeff Z0 Vp] = microstrip(w, h, Er)

eps0 = 8.85418782e-12;
mu0  = pi*4e-7;
c = 299792458;

Zf = sqrt(mu0/eps0);

Eeffn = 0;
Z0n = 0;
if 1 > w/h
    Eeffn = (Er+1)/2 + (Er - 1)*((1 + 12*h/w)^-0.5 + 0.04*(1 - w/h)^2)/2;
    Z0n = Zf*log(8*h/w + w/(4*h))/(2*pi*sqrt(Eeff));
else
    Eeffn = (Er+1)/2 + (Er - 1)*(1 + 12*h/w)^-0.5/2;
    Z0n = Zf/(sqrt(Eeffn)*(1.393 + w/h + 2*log(w/h + 1.444)/3));
end

if  1 < Er
```

```
    q = (Eeffn - 1)/(Er - 1);
else
    q = 1;
end


Eeff = Eeffn;
Z0 = Z0n;
Vp = c/sqrt(Eeffn);
```

A.3 microstrip_nlayer.m

```
function [Eeff Z0 Vp] = microstrip(w, h, Er)

eps0 = 8.85418782e-12;
mu0  = pi*4e-7;
c = 299792458;

Zf = sqrt(mu0/eps0);

Eeffn = 0;
Z0n = 0;
if 1 > w/h
    Eeffn = (Er+1)/2 + (Er - 1)*((1 + 12*h/w)^-0.5 + 0.04*(1 - w/h)^2)/2;
    Z0n = Zf*log(8*h/w + w/(4*h))/(2*pi*sqrt(Eeff));
else
    Eeffn = (Er+1)/2 + (Er - 1)*(1 + 12*h/w)^-0.5/2;
    Z0n = Zf/(sqrt(Eeffn)*(1.393 + w/h + 2*log(w/h + 1.444)/3));
end

if  1 < Er
    q = (Eeffn - 1)/(Er - 1);
else
    q = 1;
end


Eeff = Eeffn;
Z0 = Z0n;
Vp = c/sqrt(Eeffn);
```

A.4 gap_capacitance.m

```
function [Cp Cg] = gap_capacitance(w, h, s, Er)

Ceven96 = 0;
if 0.1 < s/w & 0.5 > s/w
    Ceven96 = 12*w*(s/w)^0.8675*exp(2.043*(w/h)^0.12);
elseif 0.5 <= s/w & 1.0 >= s/2
    Ceven96 = 12*w*(s/w)^(1.565/(w/h)^0.16 - 1)*exp(1.97 - 0.03*h/w);
else
    error('Ratio s/w must be between 0.1 and 1.0');
end

Codd96 = w*(s/w)^((w/h)*(0.619*log10(w/h) - 0.3853))*exp(4.26 -
1.453*log10(w/h));

CevenEr = 1.167*Ceven96*(Er/9.6)^0.9;
```

```
CoddEr  = 1.1*Codd96*(Er/9.6)^0.8;

Cp = 1e-12*CevenEr/2;
Cg = 1e-12*(2*CoddEr - CevenEr)/4;
```

A.5 RingRadiation.m

```
function EffRad = RingRadiation(Er, Eeff, Z0, L, h, f)

% Constants
mu0             = pi*4e-7;
eps0            = 8.85418782e-12;
n0              = sqrt(mu0/eps0);
c0              = 1/sqrt(mu0*eps0);

w = 2*pi*f;
k = w*sqrt(mu0*eps0);
ke = k*sqrt(Eeff);
v = sqrt(Er - 1);

A = @(theta, phi) sin((ke - k*sin(theta)*cos(phi))*L/2) ./ ...
                      ((ke - k*sin(theta)*cos(phi))*L/2);

Rv = @(theta) (1 - j*v*tan(k*v*h)./(Er*cos(theta))) ./ ...
              (1 + j*v*tan(k*v*h)./(Er*cos(theta)));

Rh = @(theta) (1 + j*v*cot(k*v*h)./cos(theta)) ./ ...
              (1 - j*v*cot(k*v*h)./cos(theta));

F = @(theta, phi) j*2*sin((ke - k*sin(theta)*cos(phi))*L/2);

r = 10*c0/f;

Etheta = @(theta, phi) j*w*mu0*L*A(theta, phi).*(Rv(theta) -
1).*cos(theta)*cos(phi)*exp(-j*k*r)/(4*pi*r) + ...
                        j*w*mu0*F(theta, phi).*(Rv(theta) +
1).*sin(theta)*tan(k*v*h)*exp(-j*k*r)/(4*pi*Er*k*v*r);
Ephi   = @(theta, phi) j*w*mu0*L*A(theta, phi).*(Rh(theta) +
1)*sin(phi)*exp(-j*k*r)/(4*pi*r);

P = @(theta, phi) (abs(Etheta(theta, phi)).^2 + abs(Ephi(theta,
phi)).^2).*sin(theta)/n0;

Pr = 2*dblquad(P, 0, pi/2, 0, pi, 1e-4);

EffRad = Pr/Z0;
```

A.6 MultiErFoam.m

```
function [P1 P2] = MultiErFoam(t, g)
% MultiErFoam.m
% Generates a 3rd-order polynomial to fit shift in resonant frequency to
% dielectric constant.
% Accepts two parameters:
% t - thickness of sample
% g - thickness of air gap
% Returns two parameters:
% P1 - vector of coefficients for first resonance fitting polynomial
```

```
% P2 - vector of coefficients for second resonance fitting polynomial.

% filename is related to thickness and gap in microns
filename = sprintf('P1P2 %d %d.mat', round(t*1e6), round(g*1e6));

if (exist(filename))
    load(filename);
else
    disp(strcat(filename, ' does not exist, calculating P1 and P2...'));
end

if (1 ~= exist('P1'))
    disp('Starting first resonance...');
    SHIFT1 = [];
    for e = 1.00:0.001:1.10
        disp(sprintf('Starting Er = %f...', e));
        tic;
        [diff fMax_air fMax_sample] = RingSandwich(e, 3.0e-4, t, g, 1);
        SHIFT1 = [SHIFT1; e diff*1e3];
        stime = toc;
        disp(sprintf('Completed Er = %f in %f seconds.', e, stime));
    end
    disp('Completed first resonance.');

    P1 = polyfit(SHIFT1(:,2), SHIFT1(:,1),3);
end

figure(1);
plot(SHIFT1(:,2),SHIFT1(:,1),...
     0:0.1:20,polyval(P1,0:0.1:20),...
    'LineWidth',2);
ylabel('\epsilon_r');
xlabel('Resonant Shift [MHz]');
legend('Simulated shift vs. \epsilon_r',...
       '3^{rd}-order polynomial fit',...
       'Location','SouthEast');
grid on;
set(gca, 'YLim', [1 1.12]);

if (1 ~= exist('P2'))
    disp('Starting second resonance...');
    SHIFT2 = [];
    for e = 1.00:0.001:1.10
        disp(sprintf('Starting Er = %f...', e));
        tic;
        [diff fMax_air fMax_sample] = RingSandwich(e, 3.0e-4, t, g, 2);
        SHIFT2 = [SHIFT2; e diff*1e3];
        stime = toc;
        disp(sprintf('Completed Er = %f in %f seconds.', e, stime));
    end
    disp('Completed second resonance.');

    P2 = polyfit(SHIFT2(:,2), SHIFT2(:,1),3);
end

figure(2);
plot(SHIFT2(:,2),SHIFT2(:,1),...
```

```
     0:0.1:40,polyval(P2,0:0.1:40),...
     'LineWidth',2);
ylabel('\epsilon_r');
xlabel('Resonant Shift [MHz]');
legend('Simulated shift vs. \epsilon_r',...
       '3^{rd}-order polynomial fit',...
       'Location','SouthEast');
grid on;
set(gca, 'YLim', [1 1.12]);

save(filename, 'P1', 'P2', 'SHIFT1', 'SHIFT2');
```

A.7 MultiTanFoam.m

```
function [P3 P4] = MultiTanFoam(t, g, e)
% MultiErFoam.m
% Generates a 3rd-order polynomial to fit shift in resonant frequency to
% loss tangent.
% Accepts three parameters:
% t - thickness of sample
% g - thickness of air gap
% e - dielectric constant of sample
% Returns two parameters:
% P3 - vector of coefficients for first resonance fitting polynomial
% P4 - vector of coefficients for second resonance fitting polynomial.

% filename is related to thickness and gap in microns
filename = sprintf('P3P4 %d %d %d.mat', round(t*1e6), round(g*1e6),
round(e*1e3));

if (exist(filename))
    load(filename);
else
    disp(strcat(filename, ' does not exist, calculating P1 and P2...'));
end

if (1 ~= exist('P3'))
    disp('Starting first resonance...');
    SHIFT3 = [];
    for d = 0:1e-5:0.005
        disp(sprintf('Starting tand = %f...', d));
        tic;
        [diff fMax_air fMax_sample BW_air BW_sample] = RingSandwich(e, d, t,
g, 1);
        Q_diff = fMax_air/BW_air - fMax_sample/BW_sample;
        SHIFT3 = [SHIFT3; d Q_diff];
        stime = toc;
        disp(sprintf('Completed tand = %f in %f seconds.', d, stime));
    end
    disp('Completed first resonance.');

    P3 = polyfit(SHIFT3(:,2), SHIFT3(:,1),3);
end

figure(1);
Q_range = min(SHIFT3(:,2)):0.1:max(SHIFT3(:,2));
plot(SHIFT3(:,2),SHIFT3(:,1),...
```

```matlab
      Q_range,polyval(P3,Q_range),...
     'LineWidth',2);
ylabel('tan\delta');
xlabel('Q Shift');
legend('Simulated shift vs. tan\delta',...
       '3^{rd}-order polynomial fit',...
       'Location','SouthEast');
grid on;

if (1 ~= exist('P4'))
    disp('Starting second resonance...');
    SHIFT4 = [];
    for d = 0:1e-5:0.005
        disp(sprintf('Starting tand = %f...', d));
        tic;
        [diff fMax_air fMax_sample BW_air BW_sample] = RingSandwich(e, d, t,
g, 2);
        Q_diff = fMax_air/BW_air - fMax_sample/BW_sample;
        SHIFT4 = [SHIFT4; d Q_diff];
        stime = toc;
        disp(sprintf('Completed tand = %f in %f seconds.', d, stime));
    end
    disp('Completed second resonance.');

    P4 = polyfit(SHIFT4(:,2), SHIFT4(:,1),3);
end

figure(2);
Q_range = min(SHIFT4(:,2)):0.1:max(SHIFT4(:,2));
plot(SHIFT4(:,2),SHIFT4(:,1),...
     Q_range,polyval(P4,Q_range),...
    'LineWidth',2);
ylabel('tan\delta');
xlabel('Q Shift');
legend('Simulated shift vs. tan\delta',...
       '3^{rd}-order polynomial fit',...
       'Location','SouthEast');
grid on;

save(filename, 'P3', 'P4', 'SHIFT3', 'SHIFT4');
```